Catalysis Science & Technology

Accepted Manuscript

ROYAL SOCIETY OF CHEMISTRY

www.rsc.org/catalysis

Catal Sci & Tech

RSCPublishing

REVIEW ARTICLE

Sailing into uncharted waters: Recent advances in the in situ monitoring of catalytic processes in aqueous environments

Cite this: DOI: 10.1039/x0xx00000x

Received ooth xxxxxx 2014,
Accepted ooth xxxxxx 2014

DOI: 10.1039/x0xx00000x

www.rsc.org/

Hui Shi,[a] Johannes A. Lercher,[a,b] and Xiao-Ying Yu*[a]

Catalysis in aqueous environments attracts enormous interest. Many characterization methods are well established at gas-solid interfaces, yet a majority of the surface-science approaches were limited to model surfaces and vacuum conditions. However, practical scenarios with complex catalyst structures, elevated temperatures and pressures, as well as the presence of two or more condensed phases, can pose immense challenges to these techniques, particularly for catalysts at their dynamic working states. In such contexts, this review highlights the advancement over the past five years in the *in situ* and time-resolved detection of catalytic processes and related phenomena in aqueous media, ideally under realistic conditions. We highlight latest technical innovations and novel chemistries that are made possible by recently developed toolboxes. Future directions of *in situ* and time-resolved analytical approaches applicable to aqueous phase catalysis are also presented.

1. Introduction

Numerous catalytic processes take place in liquids, in particular water, a green solvent and a ubiquitous fluid in many chemical and biochemical systems. Catalysis in liquid water does not necessarily proceed via the same trajectory as in the gas phase. Even if the sequence of elementary steps remains identical or similar, the energetic landscape is often impacted by the large number of surrounding water molecules, thus leading to drastic shifts in catalytic activities and selectivities. Moreover, the surface, local, and even bulk structures of the catalyst can be significantly modified in the presence of liquid water, which becomes progressively invasive at elevated temperatures. As a result, monitoring the catalytic events as well as associated physicochemical changes with the catalysts in the aqueous environment, preferably under realistic conditions and in a time-resolved manner, is pivotal for developing better understanding of reaction mechanisms and active-structure requirements of these catalytic processes, and would eventually allow rational design of efficient and robust catalysts in water.

[a] *Fundamental and Computer Sciences Directorate, Pacific Northwest National Laboratory (PNNL), Richland, WA 99352, USA. Email: xiaoying.yu@pnnl.gov*

[b] *Department of Chemistry, Technische Universität München (TUM), Lichtenbergstraße 4, D-85747, Garching, Germany.*

Despite these obvious needs, many techniques that are used to characterize catalysts and to follow catalytic reactions and related phenomena (e.g., nucleation/growth, sorption/solvation, charge transfer, surface restructuring) are typically confined to vacuum conditions, or, at best, in the presence of gas phase molecules close to ambient pressures. Without tailored cell designs and improved detection methods, they are often not practically feasible to operate in liquid water, due to either spectral interference from bulk phases or poor penetration depths in condensed phases for some probes.

A compilation of recent topical reviews on the *in situ* applications of many catalyst characterization techniques was published in a themed issue of Chemical Society Reviews in 2010, albeit with limited examples in liquid water. Latest reviews have presented, in great detail, fundamental principles of a vast variety of techniques, and provided relevant examples for studying reaction chemistries at solid-liquid (s-l) interfaces,[1] and for observing reaction progress and heterogeneities within individual catalyst particles at work by modern spatiotemporal spectroscopy.[2] None of them, however, has placed an emphasis on the application of *in situ* and time-resolved characterization tools to study catalysis in the aqueous phase.

In light of this gap, we provide a concise overview of the major developments that have occurred in the past five years with the space- and time-resolved detection of catalytic

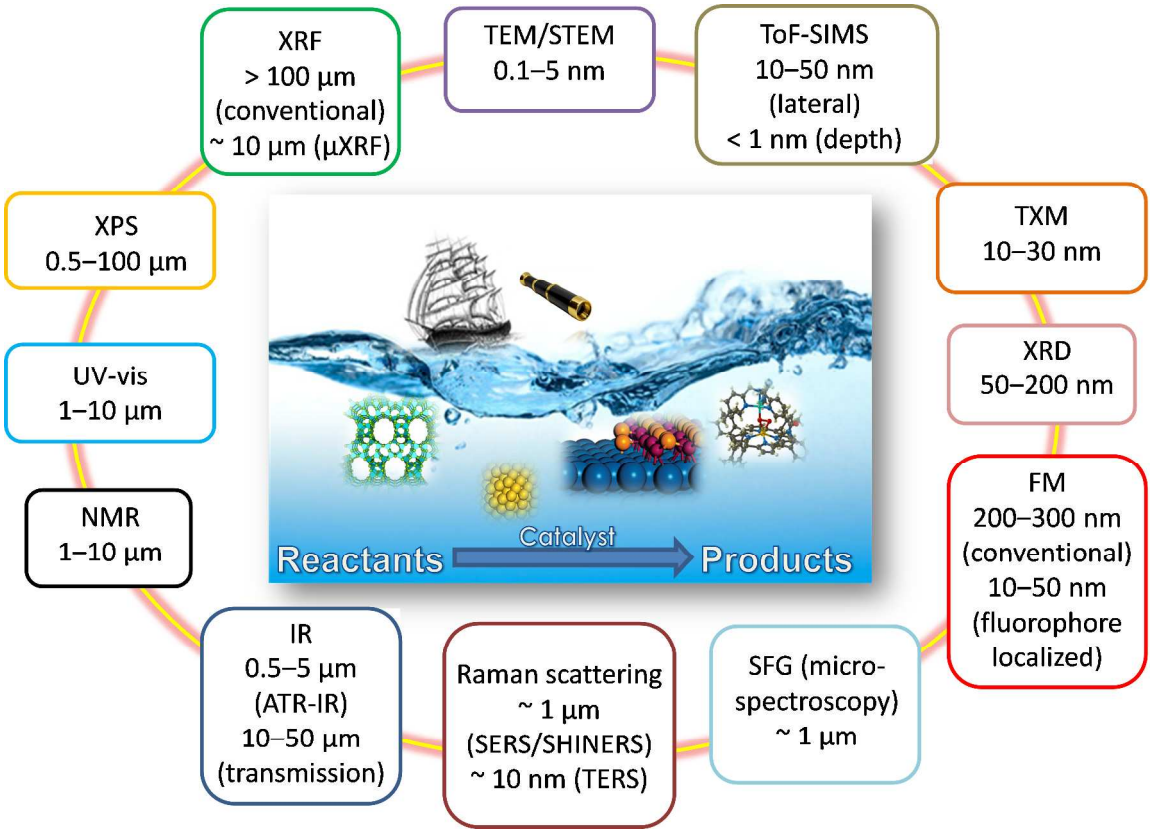

Fig. 1 *In situ* characterization techniques applicable to aqueous-phase catalytic systems, along with their typical spatial resolutions (decreasing clockwise from TEM). IR: infrared spectroscopy; ATR-IR: attenuated total reflectance infrared spectroscopy; SERS: surface enhanced Raman scattering; TERS: tip-enhanced Raman scattering; SHINERS: shell-isolated nanoparticle enhanced Raman scattering; SFG: sum frequency generation; UV-vis: ultraviolet-visible spectroscopy; XRD: X-ray diffraction; NMR: nuclear magnetic resonance; TEM: transmission electron microscopy; STEM: scanning transmission electron microscopy; TXM: transmission X-ray microscopy; FM: fluorescence microscopy; (µ)XRF: (micro)X-ray fluorescence; XPS: X-ray photoelectron spectroscopy; ToF-SIMS: time-of-flight secondary ion mass spectrometry.

processes in the aqueous phase. Throughout this review, we define "*in situ*" studies as those which apply the characterization techniques under the same environment, i.e., in *liquid* water, where the catalytic process of interest is preferably implemented. "Time-resolved" techniques follow, as a function of time, the formation and disappearance of chemical species, as far as the kinetics is concerned, or the dynamic changes in the quantity and nature of the active site, as far as the molecular or microscopic structure of the catalyst is concerned. To be rigorous, one might want to distinguish "real-time" from "time-resolved", since the temporal resolution of the characterization tool must be within the time scale of a single catalytic turnover for truly "real-time" monitoring of a catalytic reaction. Finally, an *operando* study requires that the chemical conversion be simultaneously analysed alongside spectroscopic measurements within the same reactor cell and catalyst bed.

First, we start with reviewing major vibrational spectroscopies for *in situ* interrogations into s-l (solid-aqueous) interfaces. Because these techniques are extensively reviewed, we include only technical and chemical aspects that are most relevant to the characterization of aqueous phase catalysis. Second, we focus on the applications of X-ray and solid-state nuclear magnetic resonance (NMR) spectroscopies for probing such systems under realistic conditions in heterogeneous catalysis. The next section is dedicated to typical microscopic and spectroscopic imaging approaches for acquiring temporally- and spatially-resolved information at s-l interfaces. We conclude with remarks on the present status of the field and perspectives on emerging techniques that hold great promise, yet not fully exploited, in *in situ* and time-resolved catalytic studies in the aqueous phase.

Fig. 1 summarizes the majority of *in situ* spectroscopic and microscopic techniques that are applicable to aqueous environments, along with their typical spatial resolutions. Table 1 compiles approximate time scales for the selected examples of catalytic reactions or related phenomena that occur in the aqueous phase under specified conditions, as well as the time resolutions for the interrogating techniques. Table 2 provides an overview of approximate time resolutions for each technique discussed in this review. Be aware that the reported "time resolution" is often not merely defined by the acquisition technique and instrument. Sampling period could put a limit on the reported time resolution. For example, extended acquisition may be needed to obtain useful data (e.g., increasing the number of scans in NMR to get the desired signal-to-noise ratio).

In all the examples to be discussed, the solid phase involve not only conventional catalytic solids but also colloidal

Table 1 Time scales for catalytic reactions or related phenomena in the aqueous phase and time resolutions for interrogating techniques

Catalytic reactions or related phenomena	Catalyst and conditions	Time scale of catalytic turnovers or other processes[a]	Interrogating technique[c]	Time resolution[e]	References
1. Thermal catalytic reactions					
H_2 production from HCOOH	B-doped Pd/C, 30 °C	1−10 s	ATR-IR	5 s	[3]
Glycerol reforming	Pt/γ-Al_2O_3, r.t.	~ 6 s (glycerol adsorption) 3−15 min (CO_{ads} formation)	ATR-IR	60 s	[4]
Hydrodechlorination of 1,1-dichloroethane	Bimetallic PdAu nanoshells, r.t.	> 40 min	SERS	1 min	[5]
Phenol hydrodeoxygenation	Pd/C, 35 bar H_2, 200 °C	~ 1 s	XAS[d]	2 min	[6]
Crotyl alcohol oxidation	Bimetallic PdAu, 21 °C	~ 100 s	XAS[d]	36 s	[7]
Methanol dehydogenation	Ru complexes, 86−95 °C	1−100 s	Solution NMR	Not given	[8]
C−H bond oxidation	Ir complexes, r.t.	6−100 s	Solution NMR UV-vis	1 min 5 s	[9]
Cyclohexanol dehydration	BEA zeolites, 160 °C	~ 100 s	MAS-NMR	5−10 min[f]	[10]
Reductive N-deoxygenation of resazurin	Mesoporous SiO_2-coated 2D Au nanoplates	< 1 s	FM	22 ms	[11]
2. Electrocatalytic reactions					
Oxygen reduction and evolution	MnO_x, 0.05−1.8 V (vs. RHE), r.t.	Not given[b]	XAS[d]	3 min	[12]
$Fe(CN)_6^{3-} + e^- = Fe(CN)_6^{4-}$	Au ultramicroelectrode, -0.4 − 0.4 V (vs. Ag wire), r.t.	Not given	Step-scan IR	< 1 μs	[13]
HCOOH to CO_{ads}	Pd film electrode, 0 − 0.4 V (vs RHE), 25 °C	Not given	ATR-SEIRAS	5 s	[14]
3. Photocatalytic reactions					
Water oxidation	IrO_x nanocluster, $Ru^{III}(bpy)_3^{3+}$ as oxidant, r.t.	< 160 ms	Rapid-scan ATR-IR	~600 ms	[15]
	Co_3O_4 nanoparticles, $Ru^{III}(bpy)_3^{3+}$ as oxidant, r.t.	< 300 ms (fast site) ~1 s (slow site)	Rapid-scan ATR-IR	300 ms	[16]
4. Nucleation, growth and dissolution of nanomaterials					
Formation of colloidal Au nanoparticles (NPs)	$HAuCl_4$, citric acid, PVP, 70 °C	Au_2 and Au_3 clusters (0−80 min); Au_4-Au_{13} (80−180 min); > 2 nm Au clusters (> 180 min)	XAS	~ 10−600 s[g]	[17]
Growth of zincophosphate sodalite	Seed crystal, aqueous mother liquor containing Zn, P and Na, r.t.	Not given	AFM	~ 0.25 s	[18]
PtO_2 growth on Pt NPs	Aqueous H_2SO_4 solution, 1.4 V external potential, r.t.	Pt−OH formation (0 − 10 s); Pt−O−Pt (~ 100 s)	XRD	~ 0.5 s	[19]
Metal-organic frameworks	$AlCl_3$, amino-terephthalic acid, DMF, 120−140 °C	Not given	SAXS/WAXS	10−30 s	[20]
5. Ultrafast dynamics					
Charge transfer from metal ions to water	$Co^{II}Cl(H_2O)^{5+}$, r.t.	0.6−3 fs	TFY XAS	Not given	[21]
Photo-induced substitution	cis-$[Ru(bpy)_2(py)_2]^{2+}$, UV excitation, r.t.	Not given	Pump-probe XAS	~ 100 ps	[22]

[a] Time scale was estimated from the reported turnover rate per site. [b] The typical turnover frequencies for reported biomimetic catalysts are on the order of 10^{-2} – 1 s^{-1} $site^{-1}$, translating to time scales of 1−100 s. [c] ATR-IR: attenuated total reflectance infrared spectroscopy; SERS: surface enhanced Raman scattering; XAS: X-ray absorption spectroscopy; ATR-SEIRAS: attenuated total reflectance surface-enhanced IR absorption spectroscopy; NMR: nuclear magnetic resonance; MAS: magic angle spinning; TFY: total fluorescence yield; SAXS/WAXS: small-angle/wide-angle X-ray scattering; XRD: X-ray diffraction; AFM: atomic force microscopy; FM: fluorescence microscopy. [d] In these cases, the technique was used to follow the local structural changes at the catalyst surface. [e] Note that the sampling period puts a limit to the time resolution. [f] Estimated from the number of scans and T_1 values. [g] Estimated.

nanoparticles (NPs), while the liquid phase pertain to pure liquid water, aqueous solutions, or, in a few cases, biphasic liquids containing water. Studies on catalysis-related phenomena, such as sorption and nucleation, are also surveyed when relevant. Wherever necessary, electro- and photochemical s-l interfaces are discussed in distinction from heterogeneous catalytic systems.

2. Vibrational Spectroscopies

Interface-specific vibrational spectroscopies are useful for obtaining information on the nature and concentration of adsorbates on solid surfaces. Methods based on inelastic scattering of particles other than photons, e.g., high-resolution electron energy loss spectroscopy (HREELS) and inelastic neutron scattering (INS), are not surveyed here, because they require more expensive instruments, exhibit relatively low resolution, and are often degraded by multiple scattering events in the thick liquid layers. Only techniques that detect photons in aqueous solutions are reviewed in this section.

2.1 Fourier transform infrared (FT-IR) spectroscopy

The main difficulty in using infrared (IR) radiation to study adsorption and catalysis in aqueous phase, especially species of low concentrations at surface or in solution, is associated with the marked spectral interference of liquid water itself, unless

the path length of the light is on the order of a few microns. In addition, the fundamental vibrations, as well as overtone and combination bands, of water set in from 1600 cm^{-1} in IR to 7400 cm^{-1} in near-IR region. Dependence of H-bonding with temperature can be another obstacle. These aspects were addressed in two recent reviews.[1,23]

New advances in IR absorption spectroscopy for the characterization of heterogeneous catalytic reactions are described in a recent review.[23] Here, our scope is focused on the attenuated total reflection infrared spectroscopy (ATR-IR) which has found widespread use in probing s-l interfaces and determining mechanistic aspects of aqueous phase reactions.[24] Transmission and reflection-absorption modes are mostly applicable only to either reflective solid surfaces or transparent solid samples, and often have to use thin liquid films to avoid absorption by the aqueous phase.[23]

Table 2 Typical time resolutions for the techniques discussed in this review

Probing technique	Typical time resolution[a]
ATR-IR	1−100 s (conventional);
	1 ms−1 s (rapid-scan);
	1 ns−1 ms (step-scan)
Raman scattering	1−100 s (conventional);
	1−10 fs (coherent anti-Stokes)[b]
SFG/SHG	1−10 s (conventional); 1 fs−1 ps (pump-probe)[b]
XAS	1−10 ms (energy-dispersive, DXAFS);
	1−10 s (scanning, QXAFS);
	1 fs−1 ps (pump-probe)[b]
XPS	1−10 s (conventional); 1 fs−1 ps (pump-probe)[b]
SAXS/WAXS/XRD	1−5 s (conventional); 1 fs−1 ns (pump-probe)[b]
NMR	0.1−10 s
EPR	1 s (conventional CW[c]);
	1 ns−1 μs (transient or pulsed method)
UV−vis	1−100 s (scanning);
	0.1−1 ms (single wavelength)
EM	0.1−10 s (conventional); 100 fs−1 ns (dynamic)
STM	1−10 s (standard); 0.1−1 s (scanning);
	1 ms−1 μs (atom tracking, open feedback loop);
	1 fs−1 ps (shaken-pulse-pair-excited)
AFM	0.1−10 ms (conventional);
	100 ns−1 μs (FF-trEFM[d])
FM	1−100 s (conventional); < 100 fs (Kerr-gated)

[a] Note that the sampling period puts a limit to the time resolution. [b] Pump-probe schemes help access, typically, fs to ps time scales; in addition, fast detection electronics can help access ns time scales and slower, and some other methods (e.g., time-correlated single photon counting) can help access ps time scales and slower. [c] Short for "continuous wave". [d] Short for "fast free time-resolved electrostatic force microscopy", a variant of AFM.

2.1.1 Design of the ATR-IR cell for aqueous phase experiments

For ATR-IR setups, heterogeneous catalysts are typically deposited on the internal reflection elements (IRE, e.g., ZnSe) as layers of powders or as thin films, which are then exposed to the aqueous phase reactants. A catalyst layer that is either too thick or too thin will either decrease signal throughput, or, has too few adsorption sites for detection, respectively. To be applicable to aqueous phase detection, the coated layer must also be stable enough against friction forces under static/flowing conditions, and must even, sometimes, sustain heated environments which make water chemically more invasive to many solid surfaces.

The environment within a few micrometers from the IRE is selectively probed by the evanescent IR probe wave.[25] Multiple IREs with high geometrical surface area can be used in order to improve the signal-to-noise (S/N) ratio.[26] Most recently, Si wafers with straight edges cut by simple dicing machinery or manual cleaving were demonstrated as a type of cost-effective and easy-to-prepare IRE for conducting ATR-IR spectroscopic measurements. Particularly attractive is that it creates well-defined edges without the need for polishing and laborious preparation, which generally requires deposition of a protective layer, photolithography, wet etching, and most importantly, quite accurate alignment to crystallographic directions.[27]

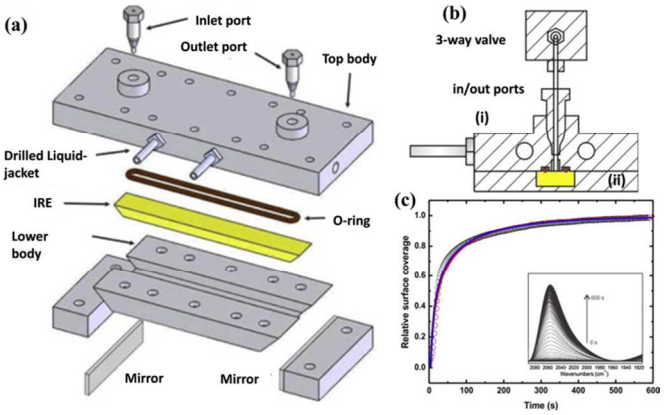

Fig. 2 (a) Scheme of the main parts of an optimized ATR cell for studying solid-aqueous (s-l) interfaces; (b) details of the entrance/exit ports, with (i) the top body with a drilled liquid-jacket to allow the control of the temperature of the cell by means of a thermostatted water bath, a cavity to host a Viton O-ring which define the height of the cell, and the inlet and outlet ports and (ii) the lower body, where the IRE is adjusted to the O-ring defining a total cell volume of 60 μL; (c) evolution of the normalized IR signal of Pt–CO (2048 cm^{-1}) as function of time upon flowing CO-dissolved liquid water over Pt (20 nm layer)-coated IRE. Blue and red lines are the best fits of the data considering different kinetic models. Adapted from ref. 26 with permission. Copyright 2014 Elsevier.

A versatile reactor design, which combines an ATR optics at the bottom to monitor the liquid phase and two transmission windows to analyse the gas phase, was presented in a recent work, where the scope of quantitative spectroscopic measurements was tested with a biphasic switchable solvent synthesis.[28] Such a design could potentially allow *in situ* ATR-IR studies of a heterogeneously catalyzed reaction in multiphasic systems involving liquid water and binary solvents containing water.

To extract time-resolved and (semi-)quantitative information on the evolution kinetics of surface intermediate species from *in situ* ATR-IR experiments, mass transport issues in the ATR cell need to be carefully precluded. Aguirre et al.[26] provided several design criteria, an analysis of the operative limits to obtain intrinsic kinetic information, and an optimized

design of a flow-through ATR cell for transient experiments at the s-l interface, by examining the case of CO adsorption in aqueous phase on Pt thin film deposited on the IRE (Fig. 2c). Linear-shaped entrance and exit ports, close to the extremes of the cell (Figs. 2a and 2b), avoid dead-volume zones (rapid-exchange without cross-contamination) and permits a uniform fluid velocity profile across the cell, which fully develops immediately after the ports.[26]

2.1.2 Probed chemistries

In situ ATR-IR studies during the past few years mainly addressed three types of systems pertaining to aqueous phase catalysis: catalytic upgrading of biomass-derived oxygenates,[3,4,29,30] electrocatalytic conversion of small organic molecules,[14,31,32] and photocatalytic decomposition or oxidation of organics in water.[33–35] These studies focused on *in situ* changes in either surface adsorbed species or functional groups during chemical transformations in liquid water. Most examples used catalyst-coated IRE; therefore, monitored adsorption/reaction at the catalyst-solution interface in the μm scale. In one of these works,[29] the sole purpose of using ATR-IR spectroscopy was to circumvent the strong interference of water absorption, and the catalyst was dispersed in the aqueous solution instead of being coated on IRE.

Among the former two types of studies, a majority have dealt with CO adsorption and oxidation over noble metal catalysts in liquid water. For instance, Copeland et al.[4] found that the rates of formation and conversion of different adsorbed CO species in aqueous phase reforming of glycerol strongly depend on the catalyst layer cleaning procedure applied prior to kinetic studies. In another study,[3] the time course of the changing stretching vibrational frequency of the bridging CO species was monitored by high-sensitivity ATR-IR in an aqueous formic acid-formate solution. The low coverage and slower accumulation of adsorbed CO, which was detected even at CO gas-phase content below 1 ppm, partly accounted for the enhanced H_2 production on boron-doped Pd/C catalysts compared to non-doped Pd/C catalysts.

By studying photo-oxidation of ethanol, acetaldehyde and acetic acid in dilute aqueous solutions over pristine and platinized P25 TiO_2, Gong et al.[33] demonstrated the feasibility of *in situ* ATR-IR spectroscopy, adapted for optical pumping, to investigate not only the reaction pathway but also the change in electronic states of the photocatalyst under *operando* conditions and its relation to activity. From their results, it was concluded that photo-mineralization of acetic acid is rate-limiting in ethanol photo-oxidation.

Most recently, ATR-IR has been used for the first time to follow *in situ* synthesis of non-surfactant-capped Au NPs in water. As Au NPs were formed and deposited at the surface of the ATR waveguide, an enhancement of the water absorption features (surface-enhanced infrared absorption, SEIRA) was observed, which correlated with the amount of NPs present at the surface.[36] Given that the Au NPs are not covalently attached to the ATR waveguide surface, this study unlocks the potential for future SEIRA-assay applications based upon the *in situ* generation and subsequent removal/renewal of the SEIRA-active layer at the waveguide surface.

2.1.3 New insights from rapid-scan ATR-IR

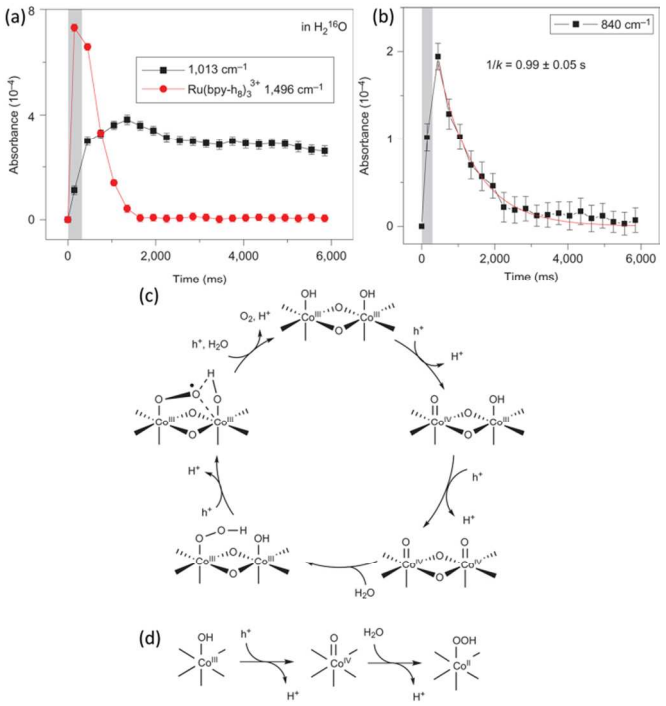

Fig. 3 Temporal behaviours of (a) 1030 cm^{-1} intermediate assigned to surface superoxide and (b) 840 cm^{-1} intermediate assigned to Co^{IV}=O. That of oxidized sensitizer Ru(bpy-h$_8$)$_3{}^{3+}$ (1496 cm^{-1}) on visible light-sensitized water oxidation at Co_3O_4 catalyst in $H_2{}^{16}O$ is also shown in (a). The duration of the 300 ms laser pulse is indicated by the grey area. Error bars represent half the peak-to-peak height of the noise level. Proposed mechanisms for water oxidation on (c) the fast Co_3O_4 surface site and (d) the slow Co_3O_4 surface site. The OO bond-forming step with H_2O in the fast cycle features the cooperative effect of adjacent electronically coupled Co(IV)=O sites, which is absent in the H_2O addition reaction at the slow site. Adapted from ref. 16 with permission. Copyright 2014 Nature Publishing Group.

In situ ATR-IR experiments reviewed above were primarily used to qualitatively track the disappearance or formation of certain surface species. A compromise between temporal resolution and S/N ratio seems inevitable. Slow kinetics on the time scale of minutes or seconds (see Table 1) can be readily followed by standard FTIR equipment, which averages signals over several scans and thus takes longer time to acquire spectra. To monitor surface species with large IR absorption coefficients, such as CO, even single scans may be sufficient to get decent S/N ratios. Apparently, faster kinetics and smaller absorption coefficients for species of interest would pose greater challenges against faster spectra acquisition, limiting the ability to average signal.[23]

Related to the above remarks, another important yet often overlooked issue arises as to the kinetic relevance of these surface intermediates in reactions. Are they so stable as to be spectators that do not participate in the catalytic cycle? Or, is it that they are involved in the cycle, but do not dictate the rates at

which the cycle turns over? In either case, the time constant of the catalytic reaction, determined from kinetic measurements, would remarkably differ from the lifetime of kinetically irrelevant chemical species, determined from the spectroscopically monitored transients.

One way to address these questions is to apply rapid-scan spectroscopic measurements with temporal resolution of sub-seconds or milliseconds. For comparisons, the average time scales with conventional ATR-IR are on the order of minutes, or, at best, of several seconds, especially when signals are not strong, whereas rapid-scan setups can move mirror at much faster velocities and obtain time resolutions on the order of tens of milliseconds.[23] The price to be paid for a higher temporal resolution will be spectral resolution, if the shorter scan time is achieved by reducing the travelling distance of the mirror.

Notably, Frei and co-workers[15] used rapid-scan ATR-IR spectroscopy to study visible light-sensitized water oxidation catalysis in aqueous solutions. For the first time, compelling evidence was presented for a surface hydroperoxide as the true reaction intermediate upon water oxidation at IrO_2 nanoclusters by recording the O–O vibrational mode at 830 cm^{-1}. More recently,[16] two surface intermediates for water oxidation, i.e., a three-electron surface superoxide and an oxo-Co(IV) species, were identified on Co_3O_4 catalysts. At a fast catalytic site, the superoxide intermediate accumulates and O_2 evolves within a 300 ms photolysis pulse. By contrast, a slow site marked by a Co(IV)=O group does not evolve beyond the one-electron intermediate within the same 300 ms pulse. The distinct temporal behaviours of the intermediates (Figs. 3a and 3b) led to the conclusion that these two intermediates belong to different catalytic sites. The widely different photocatalytic efficiency of the two types of site is attributed to the presence/absence of adjacent Co(III)OH groups coupled via a an oxygen bridge.[16]

2.1.4 A Brief Note on Step-Scan FTIR

Even faster kinetics, with as fast as sub-microsecond time resolution, are accessible by using step-scan FTIR.[23] Most recently, Burgess and colleagues reported time-resolved detection of an electrochemical process involving a ferri/ferrocyanide redox couple, with a detection limit of 10^{-14}–10^{-13} moles, by coupling synchrotron IR radiation with step-scan interferometry and an ultramicroelectrode.[13] In principle, spectroelectrochemical measurements with time resolution approaching the time constant of the cell (ca. 1 μs) can be made with the configuration described in that work.

The main hurdle for a prevalent use of step-scan FTIR is arguably the fact that the experiments need to be reproducibly repeated a very large number of times if reasonable spectral resolutions are desired. Moreover, the overall kinetic resolution of the catalytic experiments may be defined by other factors such as the excitation source (pressure or heat pulses) used to trigger the reaction, which could eventually take milliseconds.[23]

2.2 Raman spectroscopy

Unlike transmission FT-IR where water exhibits strong bands in the spectra, only weak water features are present in the Raman spectra, thus facilitating its application in aqueous systems. In general, high temperatures and pressures do not impose additional barriers on its compatibility with water.

Conventional Raman spectroscopy has been used to monitor metal oxide complexes in aqueous solutions that are employed to deposit catalytic active site precursors on high surface area oxide supports, because it is able to probe into low frequency region, e.g., < 1100 cm^{-1}, where vibrational features in solid catalysts appear.[37] UV Raman has been widely used to study *in situ* the synthesis mechanism of transition metal-containing microporous and mesoporous materials in aqueous solutions.[38] The use of UV excitation can suppress notorious interference by fluorescence and may tremendously boost the Raman signals of surface-isolated transition metal ions by the resonance Raman effect. Resonance and surface-/tip-enhanced Raman (SERS and TERS) methods were critically reviewed.[39] Some combined advanced Raman techniques have been most recently discussed.[40]

In the following, we focus on the recent progress with arguably the most useful Raman technique for *in situ* studies of aqueous phase catalysis, namely, SERS, and highlight its newest and most attractive variant, shell-isolated NP-enhanced Raman spectroscopy (SHINERS), in which Raman scattering was amplified by Au NPs encapsulated with ultrathin and extremely homogeneous shells, initially made of silica.[41]

2.2.1 Surface-enhanced Raman scattering (SERS)

Simply put, SERS takes advantage of the plasmonic resonances in metallic nanostructures to obtain significantly enhanced Raman signals of the adsorbed molecules within a few nm of the substrate surface. It allows fast and surface-selective detection with high sensitivity, down to the single molecule and single-turnover level,[42] thus enabling real-time observations of catalytic reactions.[43] The distance-dependent decay of the SERS effect also allows observations with enhanced detail in the interfacial region.[39]

A critical choice of the SERS substrates needs to be made in terms of enhancement factors[44] for *in situ* studies of catalysis in water. In recent years, there is an emerging interest in developing new classes of plasmonic colloids that are water-compatible, e.g., multi-metallic plasmonic colloids[43,45–47] or nanohybrids,[48] as well as a desire to expand the light scattering and absorption properties of Au or Ag NPs.[49] Different from these approaches based on composite nanostructures, Joseph et al. used simultaneously immobilized Au (40 nm) and Pt (2 nm) NPs, as the plasmonic and catalytic component, respectively.[50] Abundant, non-noble or even more electronegative metals (e.g., Cu, Al, Ga), with potentially applicable localized surface plasmon resonance (LSPR), appear economically advantageous. However, associated problems include relatively high oxidizing tendency and the lack of synthetic strategies that provide precise structural control similar to that of the colloids based on noble metals.[49]

Only a handful of examples exist in regard to the *in situ* SERS monitoring of heterogeneous catalysis in water.[5,50,51] Notably, Heck et al. studied catalytic hydrodechlorination of 1,1-dichloroethene in water by *in situ* SERS on Pd islands grown on Au nanoshell.[5] Several intermediates, including π and di-σ bonded species, vinylidene, and other oligomeric moieties, involved in the dechlorination and hydrogenation steps were identified. Au substrate was found to enhance not only the Raman signal but also the catalytic activity of Pd. In a more recent work,[51] the same group followed the aqueous-phase reaction of glycerol oxidation catalyzed by Au nanoshells (on Si wafer) at room temperature (Fig. 4). Glycerate surface species, with persistent sharp peaks at ~1000, 1200, and 1500 cm^{-1}, formed very rapidly when oxygen was present, suggesting that free glycerolate reacts directly with adsorbed O_2 or surface bound OH activated by the electron scavenging O_2. Based on the SERS analysis of CO chemisorption on Au nanoshells, they concluded that higher pH values progressively weakened the C–O bond as the Au negative charge increased.

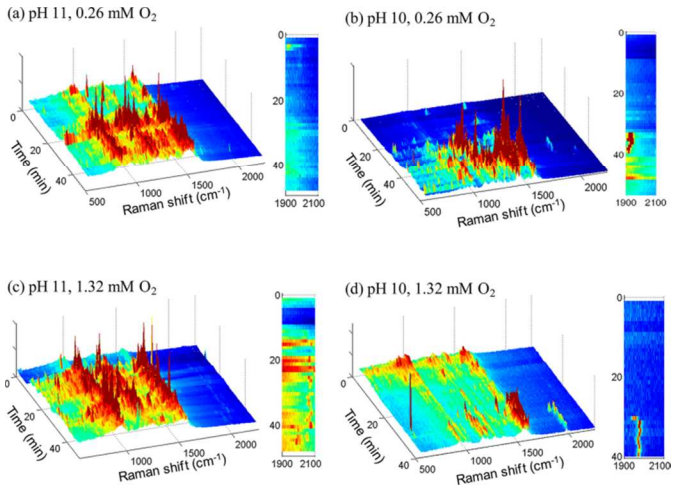

Fig. 4 Time-resolved Au nanoshell-based surface enhanced Raman spectra of 1.3-mM glycerol solutions (a) at pH 11 with 0.26 mM O_2, (b) at pH 10 with 0.26 mM O_2, (c) at pH 11 with 1.32 mM O_2, and (d) at pH 10 with 1.32 mM O_2. Reproduced from ref. 51 with permission. Copyright 2013 American Chemical Society.

The interference of the SERS substrate with the catalytic material studied, however, can be problematic. In particular, when acquiring SERS spectra during an electrochemical (EC) reaction, electrical contacts between the SERS probe (e.g., Au) and the underlying electrode (e.g., Pt) can lead to SERS signals and electrocatalytic performance that are not solely related to the electrode material. A most recent approach to tackling this interference is to use self-assembled monolayer (SAM) of 11-mercaptoundecanol that insulates the Pt electrode from the SERS-active gold microshell which would otherwise participate in EC reactions as a part of the electrode.[52] Key to this approach is an appropriate length of the SAM to ensure electrical insulation and little decay in SERS intensity, while hardly influencing the EC reaction.

So far, only limited success has been reported on *in situ* SERS studies of catalytic reactions in the aqueous phase at elevated temperatures. When probing such reactions, thermal and chemical robustness is a prerequisite for the SERS substrate. Ultrathin metal oxide overlayers deposited by atomic layer deposition may serve to stabilize the substrate against annealing.[39]

2.2.2 Shell-isolated nanoparticle-enhanced Raman spectroscopy (SHINERS)

Since its invention in 2010,[41] SHINERS has attracted tremendous attention, mainly from the analytical community. The key for the SHINERS method is the synthesis of special core–shell heterostructures with a SERS-active core and a shell that is inert, compact, and ultrathin. The size of the core can range from 50 up to 120 nm, with sphere, cube or rod shapes currently possible.[53] The shell materials can be SiO_2, Al_2O_3, MnO_2 and Ag_2S, tailored for different pH environments. Typically, the shell thickness should be less than 3 nm and pin-hole free.[53] Compared with TERS, where only a few molecules located in the nanosized gap between tip and single crystal surface are sampled, the total number of Raman scattered photons is much larger in SHINERS.[54] In exchange for the increased sensitivity in this manner, however, the price is a loss of spatial resolution in SHINERS compared with TERS (Fig. 1). Besides the high detection sensitivity, the main virtues of this technique also include effective protection of the SERS-active nanostructure from direct contact with the probed adsorbates and practical applicability in materials with diverse morphologies. These features eliminate distortion of the true vibrational information and meet the research needs in the *in situ* and time-resolved study of heterogeneous catalysis and electrocatalysis in aqueous environments. In addition, SHINERS can probe the spectral changes of low-frequency modes (< 400 cm^{-1}),[55] inaccessible to standard FTIR techniques using KBr optics and standard MCT/InSb/DTGS detectors.

Two recent reviews were published on the application of SHINERS in electrochemistry.[53,56] Intermediates during EC processes, such as SCN^-, pyridine, CO and H on single crystal Au, Pt and Rh electrodes, have been examined, all in aqueous solutions. Although surface plasmon (SP) coupling between Au NPs has long been considered more efficient than the coupling between NPs and a smooth surface, it was surprisingly found that SHINERS intensity is comparable to, or several times greater than, the SERS intensity.[54]

Most recently, an all-optical probing technique of local chemical reactions based on single shell-isolated Au NPs was demonstrated using H_2 uptake in Pd as a model system.[57] The Au core concentrates strong electromagnetic near-fields into a subwavelength volume adjacent to the Pd film and report, in real-time, the local subtle environmental changes at its pinning site during H_2 uptake through the dielectric changes of Pd with different shell thickness and at varying H_2 concentrations (Fig. 5). Remarkably, the spectral response shown in Fig. 5c shifts completely to the opposite direction compared to that in the particle-on-film platform (Figs. 5a and 5b), underlining the suitability of this technique for studying local reactions on

surfaces with various morphologies. Though the study was conducted at gas-solid interfaces, the nano-optical technique and single particle platform have clearly demonstrated the potential to be applied to a plethora of chemical reactions at s-l interfaces.[57] Finally, we remark that the potential of the SHINERS technique has not been fully unlocked in catalysis, in such directions as quantitative determination of surface coverages on powder-form heterogeneous catalysts.

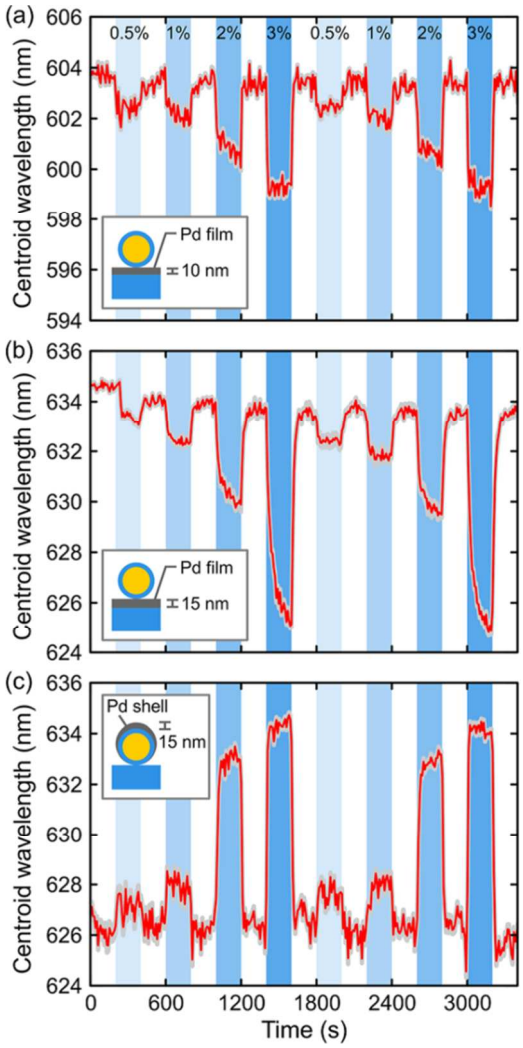

Fig. 5 Experimental time-resolved centroid wavelengths in response to H_2 uptake and release. (a) Single shell-isolated particle on a 10 nm Pd film. (b) Single shell-isolated particle on a 15 nm Pd film. The minute 5 nm film thickness change can easily be resolved optically under the same reaction conditions. (c) Single shell-isolated particle covered by a 15 nm Pd film. The statistical error (standard deviation) of the calculated centroid wavelengths is below σ = 0.13 nm in all cases. Reproduced from ref. 57 with permission. Copyright 2013 American Chemical Society.

2.3 Second order non-linear optical spectroscopy

Both sum frequency generation (SFG) and second harmonic generation (SHG) originate from second-order non-linear two-photon processes. Both techniques are highly interface-specific, (sub)monolayer-sensitive, and can shed light on the molecular orientation at the interface; they are extensively reviewed.[58] Here, the s-l interface is the most pertinent.

There are only a few *in situ* investigations that used SFG/SHG spectroscopy to study adsorption of molecules on colloidal particles in water[59] or oil-in-water emulsions;[60] none have been reported to probe into the kinetics of a heterogeneous catalytic reaction in liquid water. Notably, You et al.[60] monitored in real-time (~1 s time scale) the transfer of SHG-active surfactant molecules from a donor emulsion droplet to an acceptor emulsion droplet, and found that an increase in the hydrophobic chain length, from 1-butyl to 1-octyl, decreases the transfer rate by 600 times. These results may have important implications on phase transfer catalysis in oil-in-water emulsion systems.

2.3.1 Applications to electrocatalytic systems

A majority of recent applications of SFG/SHG spectroscopies for monitoring catalysis in water are found in EC systems. As both the electrode and aqueous electrolyte are strong IR absorbers, *in situ* spectro-EC experiments were often performed in an EC cell containing a well-defined thin layer (typically a few tens of μm, established by, for example, a Teflon spacer of the same thickness) of electrolyte solution between the electrode and the optical window.

As a most recent example, Kutz et al.[61] reported the first broad-band SFG spectra of adsorbed acetate and co-adsorbed (bi)sulfate anions (when the supporting electrolyte was H_2SO_4) during electro-oxidation of ethanol on Pt electrode. A comparison of potentiodynamic SFG spectra and voltammetric data in two supporting electrolyte, H_2SO_4 and $HClO_4$, suggested that (bi)sulfate anions, but not perchlorate anions, block adsorption sites on the Pt surface and, therefore, inhibit ethanol oxidation, further implying a lower CO coverage and a significantly reduced reaction efficiency.

As remarked by Liu and Shen,[62] however, even for such a thin-layer approach, the IR input would still attenuate before reaching the electrode-electrolyte interface, and it might be difficult to separate signals originating from multiple boundaries, making extraction of the spectrum of the interface ambiguous and unreliable. In their latest contribution,[62] the authors ingeniously employed an SP wave to enhance SFG signals at EC interfaces, using the geometry shown in Fig. 6a, where the IR input excites the SP wave at the interface and overlaps with the visible input to generate the surface-specific SF output. The advantage is two-fold: 1) one can benefit from the IR field enhancement due to SP resonance; 2) because the IR field of SP is narrowly confined to the Au/water interface, the complications caused by using thin cells can be avoided.[62] By monitoring cyclic voltammetry (CV) and *in situ* SP-SFG vibrational spectroscopy simultaneously, they obtained direct evidence that long-chain thiols desorbed by reductive reactions could actually remain orderly arranged near the electrode, whereas desorbed molecules by oxidation diffuse away from the electrode after desorption (Figs. 6b and 6c), thus resolving a long-standing controversy concerning the form in which the

desorbed thiol monolayer appears in the electrolyte. This study ushers in a new era for the SFG to measure *in situ* and time-resolved interfacial vibrational spectra during electrocatalytic reactions and, by extension, other catalytic reactions at s-l interfaces.

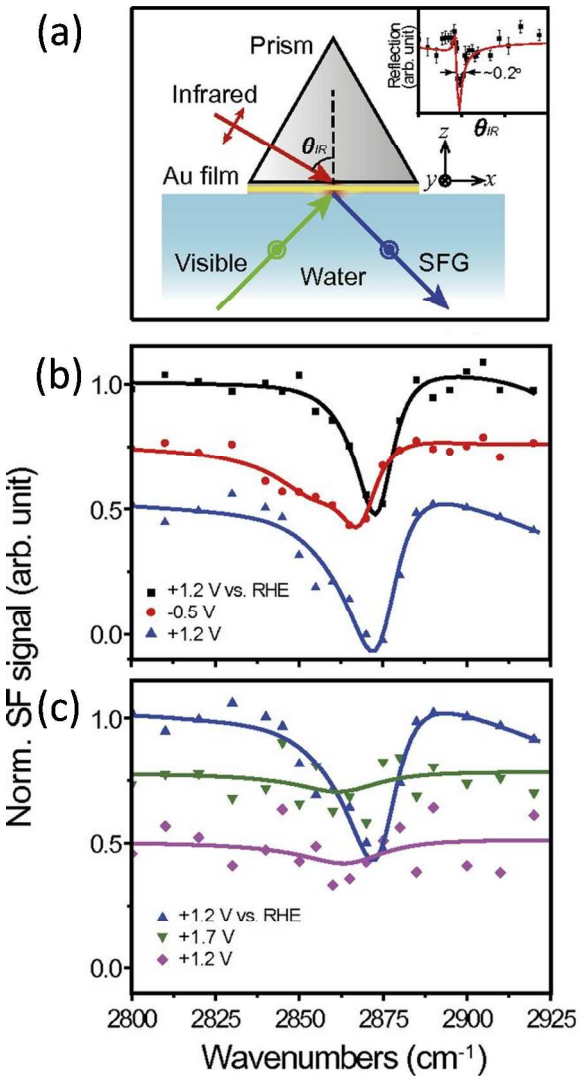

Fig. 6 SP-SFG setup and *in situ* SP-SFG of EC desorption and re-adsorption of a thiol-SAM-covered on a gold electrode in 10 mM KOH aqueous solution. (a) Schematic of experimental arrangement. The inset shows reflection of IR input at 3300 cm^{-1} from the prism-gold-air interface as a function of incident angle, with the sharp dip (FWHM ~0.2°) indicating SP resonance. Dots are measured data, and the solid curve is from calculation. (b) SFG spectra, with contributions of the Fresnel coefficients removed, from the Au/electrolyte interface, taken sequentially at different voltages during the CV scan. Plots are vertically shifted for clarity, and curves are theoretical fits. The upper two spectra were taken at the beginning and end of the cathodic scan, and the lowest one at the end of the anodic scan. (c) SFG spectra of the same interface taken at three different potentials during a scan: at +1.2 V (blue) before the occurrence of oxidative desorption of thiols, at +1.7 V (green) after near-completion of oxidative thiol desorption, and back at +1.2 V (violet) with no indication of thiol readsorption. Adapted from ref. 62 with permission. Copyright 2014 National Academy of Sciences, USA.

2.3.2 Remarks on the lack of real-time and quantitative SFG/SHG studies of practical heterogeneous catalysts

Reflective substrate surfaces have been prevalently used in SFG/SHG studies of catalytic processes in water. Significantly fewer reports use porous materials and NPs. Typically, powder catalyst samples or colloidal particles (nm to μm in size) need to be coated onto the optical substrate as a thin and optically flat film, by electron beam evaporation,[63] atomic layer deposition,[64] or the much simpler evaporation-driven self-assembly process.[65] Analysis is often aided by curve fitting, due to mediocre or poor S/Ns compared with those obtained on flat surfaces, especially in dilute aqueous solutions.[63] To enhance SFG signals and minimize destructive interference for particles with dimensions much smaller than the wavelength of light used, total internal reflection (TIR) geometry is recommended by some, but may suffer from unintended complications due to its high sensitivity to the effective index of refraction of catalyst pellets which is, in turn, affected by the adsorbate molecules.[66]

Quantitative analyses of the surface coverage and time-constant of the heterogeneous catalytic process remain scarce in the aqueous phase, partly because the SFG signals are not solely related to the interfacial concentration, but are also affected by the average orientation, molecular ordering, resonant/non-resonant components, among others. Detailed knowledge about these factors is required to derive reliably the temporal changes of the number density at the interface for a rigorous kinetics evaluation.

3. X-Ray Core-Level Spectroscopies

X-rays act as powerful probes in condensed phases and buried interfaces due to their relatively large penetration depth, which is very helpful to *in situ* studies performed in the aqueous phase. A voluminous review appeared last year that presented a collection of case studies where the use of *in situ* X-ray absorption and emission spectroscopies (XAS and XES) helps improve understanding of the structure and reactivity of surface species in heterogeneous catalysis. The creation of a core hole by excitation is studied in XAS while the creation of a core hole by ionization forms the basis for X-ray photoelectron spectroscopy (XPS). Notably, the liquid microjet, or similar techniques such as droplet trains or supported droplets, has been most widely used in XPS for studying aqueous solutions and interfaces in vacuum.

3.1 X-ray absorption spectroscopy (XAS)

XAS, or X-ray absorption fine structure (XAFS), provides an extremely powerful tool for the elucidation of chemical state and local structure of solid catalysts, particularly when powder X-ray diffraction and transmission electron microscopy (TEM) fall short in resolution for catalyst samples containing small domains and non-crystalline structure of the active component. An X-ray absorption spectrum is typically divided into two regimes, X-ray absorption near-edge spectroscopy (XANES) and extended X-ray absorption fine-structure spectroscopy (EXAFS). Unless the particle size is small enough (< 2 nm), XAS primarily probes the bulk rather than the surface fraction.

While standard XAS setups acquire data in step scan mode where the technical time resolution is on the order of 10^2 s,[67] time-resolved XAS (not including the truly "real-time" pump-probe scheme as we discuss later) was developed in energy-dispersive (1 ms time resolution[67]) and energy-scanning, or quick XAFS (QXAFS) modes (1 s time resolution[67]); the pros-and-cons of both modes are discussed in detail.[67,68] There are few inherent limits on XAS measurements that can be done in the aqueous phase and realistic conditions; however, since the characteristics of synchrotron sources and experimental station dictate what energy ranges, beam sizes, and intensities are available, practical experimental constraints do exist. Under some circumstances, the beam flux has to be lowered, by defocusing and/or filtering the beam with Kapton filters and stirring the sample, to avoid photo-induced damages (reduction, decomposition, etc.) to the local structures and self-absorption problems.[69] Experimental setups, including *in situ* and operando cells, for hard and soft XAS measurements have been reviewed;[67] we detail below the use of XAS techniques in recent catalytic studies in aqueous solutions.

3.1.1 Applications to heterogeneous and colloidal catalysis in water

Thermodynamic endpoints and kinetically (meta-)stable states of the active component can be very different in gaseous and aqueous media, so a direct, *a priori* transfer of conclusions from one system to another (e.g., oxidation of alcohols on metals in gas-phase and in water) should be avoided. However, only a few *in situ* or *operando* XAS studies dealt with heterogeneous catalysis in the aqueous phase[6,7,69–73] compared to the gas phase.

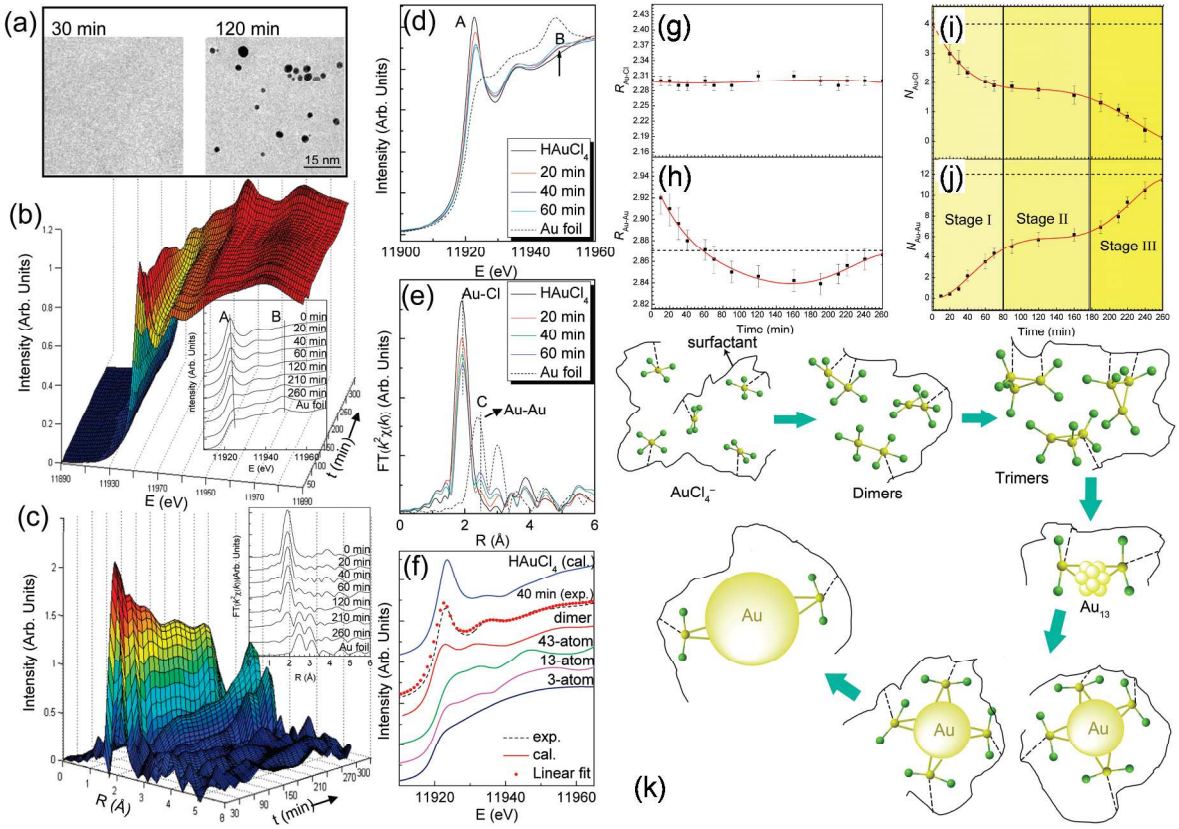

Fig. 7 (a–c) Dynamic nucleation and growth of Au NCs studied by *in situ* XAFS: (a) TEM images of Au NCs obtained at 30 and 120 min; (b) evolution of normalized Au L_3-edge in situ XANES and (c) k^2-weighted EXAFS Fourier transforms (FTs) spectra. The insets show the typical Au L_3-edge XAFS spectra at different reaction times. For the purpose of investigating the nucleation process fairly, several typical data are compared in XANES (d) and the corresponding FTs (e) spectra. (f) XANES calculations for various Au clusters, where the structural model of the naked Au_n^0 cluster adopts the most stable configurations and the dimer is assumed as the $^-Cl_3Au\text{-}AuCl_3^-$ model arising from two partially reduced $AuCl_3^-$ ions connected via Au-Au bond. (g–j) Time profiles of various structural parameters from the EXAFS fitting: the bond distance for Au-Cl (g) and Au-Au (h) and the coordination number for Au-Cl (i) and Au-Au (j) bonds. The dashed lines are noted as the corresponding values of reference $HAuCl_4$ and bulk Au. (k) A schematic representation of the formation process of Au NCs. The coiled line represents the surfactant. The formation of dimers and trimers can be classified into stage I. For the small Au clusters in stage II, the representative Au_{13} cluster is shown. In stage III, the large Au nanocrystals are produced. Adapted from ref. 17 with permission. Copyright 2010 American Chemical Society.

A recent *in situ* XAS study addressed the state of supported Pd NPs (~ 3 nm), in the aqueous phase for the first time, during various stages of catalyst conditioning and catalytic action (hydrodeoxygenation of phenol).[6] XAS analyses showed that the Pd was present initially as Pd core/PdO shell entities but the oxide shell was almost completely reduced under 35 bar H_2 within 6–10 min during the heat-up to 200 °C in water or dilute aqueous H_3PO_4 solutions. Water, dilute acids, organic

substrates, or catalyst supports were unequivocally shown to hardly affect the average size and dynamic structure of reduced Pd particles until the end of the reaction, as indicated by the essentially identical EXAFS parameters.

Similarly, Dreher et al. observed via *operando* EXAFS that in the presence of methanol, ethanol or acetaldehyde, a fresh Ru/C catalyst was reduced to its metallic, active form at around 125 °C without a change in particle size.[73] Noteworthily, a full structural analysis was performed by *in situ* XAS even in supercritical water.[74]

XAS can also be used to study *in situ* formation of colloidal metal NPs,[17,75,76] their surface oxidation (e.g., Fe[69]) and catalyzed reactions[7] in water. For example, using continuous liquid-flow *in situ* XAFS spectroscopy, Yao et al. determined the initial nucleation kinetics of Au clusters with size less than 1 nm reduced from the $AuCl_4^-$ in the aqueous solution.[17] The analysis of XAFS data (Fig. 7) indicates that, under moderate conditions, the partially reduced $AuCl_3^-$ anions would be combined through the slightly elongated Au–Au bond to form the one-dimensional "Au_nCl_{n+x}" complex clusters, from the polymerization of linear "$(AuCl_3^-)_2$" dimers, rather than to form Au_n^0 clusters from the aggregation of Au^0 atoms. The same group reached similar conclusions with Pt nanoclusters, and further uncovered that nucleation pathways can be selectively tuned by the strength of reductant, affecting in turn the post-growth dynamics and the final morphologies.[76] In a most recent study,[7] the Pd(II) salt/Au NPs-catalyzed oxidation of crotyl alcohol in aqueous solutions was followed by *in situ* (36 s per scan) XAS at both the Pd K- and L_3-edges. Several important conclusions, regarding the reduction kinetics of $PdCl_4^{2-}$ on Au NPs and the stability of Pd entities on Au against re-oxidation, were drawn from these XANES and EXAFS results. It is expected that QXAFS or dispersive XAFS modes with significantly better time resolutions (10^{-3}–1 s) would unveil more details on the dynamic changes in chemical states and local environments of the catalytic centers during reactions in water.

3.1.2 Applications to (photo-)electrocatalysis in water

Catalytic materials, in replacement for pure Pt, for the (photo-)EC oxygen reduction reactions (ORRs) and oxygen evolution reactions (OERs), based on Co,[77–79] Pt-Co,[80,81] Mn,[12,82] Ni,[83] are being actively studied by XAS during electrocatalytic turnovers. Surprisingly, the results can sometimes contrast observations under *ex-situ* conditions.[77] Unprecedented insights into the active redox couples and local chemical environments under working conditions have been acquired from these studies.[12,77–84]

For instance, coulometric measurements combined with XANES spectra of a nickel borate OER catalyst showed that the Ni centers in anodic-activated films possess an average oxidation state of +3.6, indicating that a substantial proportion of Ni centers exist in a formal oxidation state of Ni(IV), in contrast to a predominant presence of Ni (III) (β-NiOOH) in nonactivated films; these unprecedented findings challenge the general consensus that the β-NiOOH phase delivers more efficient OER catalysis.[83]

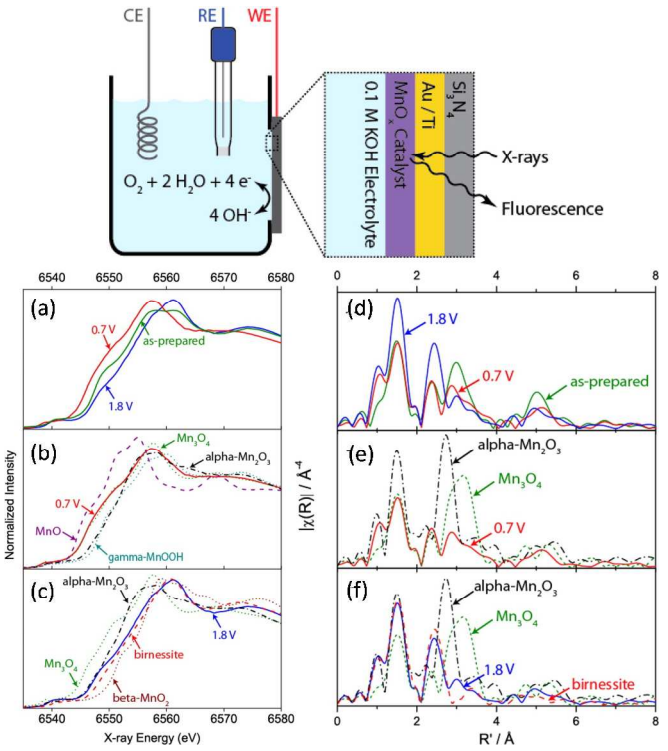

Fig. 8 Top panel: *in situ* XAS setup, with the back side of the Si_3N_4 window facing the X-rays and the front side of the window with electrodeposited MnO_x on a layer of Au/Ti facing the electrolyte. CE, RE, and WE stand for counter, reference, and working electrodes, respectively. Left below: (a) Comparison of XANES data collected on as-prepared MnO_x/Au–Si_3N_4 film and on MnO_x/Au–Si_3N_4 film after *in situ* exposure to ORR (0.7 V) and OER (1.8 V) relevant conditions. (b) MnO_x/Au–Si_3N_4 film poised at 0.7 V overlaid with MnO, Mn_3O_4, α-Mn_2O_3, and γ-MnOOH. (c) MnO_x/Au–Si_3N_4 film poised at 1.8 V overlaid with Mn_3O_4, α-Mn_2O_3, birnessite, and β-MnO_2. Right below: (d) Comparison of *in situ* EXAFS collected on as-prepared MnO_x/Au–Si_3N_4 film and on MnO_x/Au–Si_3N_4 film after *in situ* exposure to ORR and OER potentials. (e) MnO_x/Au–Si_3N_4 film poised at 0.7 V overlaid with Mn_3O_4 and α-Mn_2O_3. (f) MnO_x/Au–Si_3N_4 film poised at 1.8 V overlaid with Mn_3O_4, α-Mn_2O_3, and birnessite. Adapted from ref. 12 with permission. Copyright 2013 American Chemical Society.

Two in-depth XAS studies during ORR and OER catalysis are noteworthy, one on a tetranuclear Mn cluster[82] and the other on mixed Mn oxides,[12] both as functional mimics of the Mn-containing water-oxidation center of Photosystem II in nature. For *in situ* XAS during EC tests, fluorescence spectra, rather than transmission spectra, were recorded.[12] Mn oxidation states were observed from XANES to decrease or increase under ORR or OER conditions, respectively, indicated by the edge shifts (Fig. 8). The observed Mn valence in the catalyst during the ORR closely matches that in $Mn_3^{II,III,III}O_4$; MnO_x catalyst at OER potentials is between +3 (α-Mn_2O_3) and +4 (β-MnO_2), and exhibits strong similarity to the birnessite phase. The EXAFS spectra of MnO_x/Au−Si_3N_4 shed further light on the relevant phases; $Mn_3^{II,III,III}O_4$ formed at the ORR relevant potential is a disordered phase with smaller fitted coordination numbers. *In situ* XANES were also employed to study film porosity to understand whether OER catalysis is limited to the top geometric layer of a dense film (100–200 nm), or occurs

throughout the catalyst layer of a porous film.[12]

Most recently, Salmeron and co-workers developed *in situ* XAS recorded in total electron yield (TEY) mode to study the effect of EC reactions on the structure of graphene in aqueous electrolytes.[85] Traditionally, XAS measurements of graphene have been carried out in ultra-high vacuum. The TEY detection provides interface sensitivity due to the short mean free path of the secondary electrons (~nm), thus providing a new tool for spectroscopic studies of electrode/electrolyte (s-l) interfaces, i.e., the Helmholtz layer region. In contrast, while the fluorescence detection mode is appropriate for studies of the chemistry of the electrode materials, the signal obtained is bulk sensitive due to the large penetration depth of soft X-rays (~μm). This benchmarking study shows that the surface structure of CVD-grown graphene changes appreciably (and reversibly) at potentials below |1| V, and that defects increase dramatically (and irreversibly) at potentials above |1| V in aqueous electrolytes.[85] Unfortunately, these results were not obtained during CV scanning; in the current implementation, TEY signal is superimposed to the large Faradic current between the working electrode (WE) and counter electrode (CE) which saturates the current pre-amplifier, preventing one from collecting spectra while the EC bias is being applied.

3.1.3 Applications to homogeneous catalysis in water

Though less often employed, XAS is also an important tool, especially under *in situ* or *operando* conditions, for studying water-soluble compounds that deliver efficient homogeneous catalysis.[86,87] Desired characteristics for general-purpose XAS cells, and an exemplary design, for such studies are discussed in detail by Nelson and Miller.[88] A recent example is one that used EXAFS to detect the increase of Cr−O distance upon coordination of Cr(III) cation with the glucose molecule, a step essential for the aldose-ketose isomerization catalyzed by Lewis-acidic $CrCl_3$ together with Brønsted-acidic HCl in water.[87]

Picosecond XAS studies on monitoring excited state dynamics of transition metal complexes (e.g., intramolecular and subsequent intermolecular structural rearrangements), due to the metal-to-ligand-charge-transfer in aqueous systems, are highly relevant to a variety of catalytic and photo-induced processes.[22,89] Some charge transfer processes proceed on even shorter, femtosecond time scales (i.e., core-hole lifetime for 3d transition metals) and are currently very challenging to be reliably investigated by picosecond-resolution pump-probe measurements.

Scanning the L-edges of 3d transition-metal ions and complexes at high concentrations in the aqueous solution, Aziz et al. recently reported the so-called "dark channel fluorescence yield" method to study bonding and electron transfer between metal ions and water.[21,90] However, it remains disputable as to whether the dips observed in the 3d-transition metal L-edge total fluorescence yield (TFY) spectra are due to charge transfer (from metal to water) effects, or solely to X-ray optical effects.[91] Settling the debate will likely help advance the understanding of the electronic interaction of solutes (particularly transition metal ions) with their environment in solutions (water and other solvents) and also in heterogeneous media, such as at s-l interfaces.

As femtosecond time domains are becoming accessible now, studies of fluorescence lines with extremely low yield are being enabled by a new generation X-ray source (i.e., free-electron lasers as will be mentioned later). With that, the research on ultrafast structural chemical dynamics of homogeneous photocatalysts in water will come into full bloom.

3.1.4 Technical remarks on the *in-situ* XAS studies in water

To obtain a good sensitivity, concentrations of the metal needed for aqueous XAS measurements can be much higher (> 10 times) than those for catalytic studies. In the case of colloidal solutions, preparation of concentrated samples can lead to unintended sintering and, consequently, a larger polydispersity in particle sizes.[7] One solution is to employ fluorescence detection, which record the light emitted from a sample as a function of the incident photon energy, at very low concentrations or in low-energy measurements; for such measurements at the lowest absorption energies, the cell can be further modified by cutting a hole in the cell body and adhering a Kapton window by expoxy.[88] Spectral sharpening can be achieved in high-energy resolution fluorescence detected (HERFD) XAS by selectively detecting a fluorescence decay channel which has a core hole with a longer life-time and, thus, less broadening.[92] As mentioned earlier, the beam flux needs to be tuned in order to minimize beam-induced reversible and/or permanent changes to the samples.[69]

To perform time-resolved analyses of kinetics of most surface events, the experimental setup requires innovative designs of sample cells and improved monochromators. The newest version of eccentric cam-driven monochromators allow for much larger spectral ranges than previously used piezo-driven ones; it can collect EXAFS data with a time resolution as fast as a few tens of milliseconds per spectrum.[68] Of particular interest is the improved time resolution for dynamic XAS studies of the surface events on the Pt/C cathode in a fuel cell under operando conditions, by using the time-gating energy-scanning or quick XAFS (TG-QXAFS, 1 s) and energy-dispersive XAFS (DXAFS, 4 ms) modes developed by Iwasawa and co-workers.[93] It is noteworthy that due to the μm-dimension of the polychromatic beam at the focus point of a dispersive EXAFS setup, sample homogeneity becomes a much more critical problem than in standard step-scan or quick-EXAFS acquisitions, where the beam probes a much larger area (millimeter dimension) of, for example, a supported metal catalyst sample. In this respect, we refer to a detailed study by Newton for some limiting parameters that need to be addressed

Chem Soc Rev

RSCPublishing

REVIEW ARTICLE

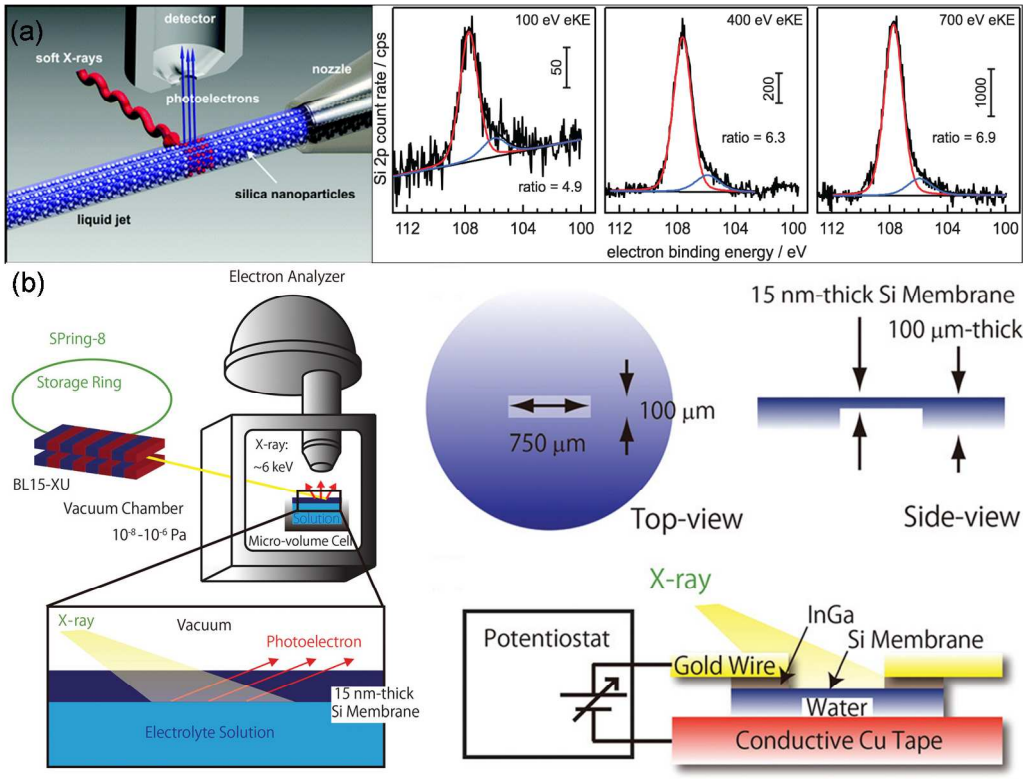

Fig. 9 Two design concepts for aqueous-phase XPS: (a) the experimental setup and Si 2p spectra for *in situ* XPS at the s-l interface of aqueous colloidal SiO_2-NPs. The 24 μm liquid jet is inserted into vacuum where it spatially overlaps with the micro focus of the soft X-rays;[104] (b) a schematic illustration of *in situ* EC XPS apparatus using hard X-rays at the synchrotron beamline (bottom left) and Si membrane and the whole XPS cell (bottom right).[107] Adapted from refs. 104 and 107 with permission. Copyright 2013 Royal Chemical Society and American Institute of Physics.

in making a successful dispersive EXAFS experiment on heterogeneous catalysts.[94]

The most recent experimental and theoretical developments in X-ray spectroscopies for time-domain studies were reviewed in 2014.[95] High repetition rate femtosecond X-ray spectroscopies represent the most eye-catching advance; these ultrafast spectroscopic methods by means of pump-probe schemes hold great promise in identifying short-lived reaction intermediates and have been applied to *in situ* studies of photo-induced charge transfer phenomena in aqueous solutions.[89] Although there have not been reports on the use of ultrafast pump-probe X-ray techniques to monitor in real time bond breaking and making events during catalytic processes in aqueous solutions, a most recent work showed that pump-probe X-ray fluorescence spectroscopic techniques based on a free-electron X-ray laser can be used to probe, on a picosecond scale, the electronic structure of a transiently populated, weakly adsorbed state in CO desorption from Ru(0001).[96]

It is worth noting that rigorous exclusion of ubiquitous diffusional limitations at multiple phase boundaries[97] needs to be made, when *in situ* XAS studies are performed in a system involving gas, solid and aqueous phases. Additionally, in the presence of gas-phase co-reactant (e.g., H_2, O_2), working with catalyst pellets or a pressed wafer in liquid water can pose the disadvantage of long (pre)-treatment times necessary to attain equilibrated adsorption on the catalyst surface and uniform distribution across the solution of gaseous co-reactants, due to diffusional limitations. A modified design was to use a catalyst with a typical powder diameter of 20 μm first treated in the slurry phase and transferred to the EXAFS cell where it settles as a packed catalyst bed of sufficient uniformity.[98]

3.2 X-ray emission spectroscopy (XES)

XES is complementary to XAS in that it probes the *occupied* density of electronic states of a material and furnishes information on the electronic structure, charge/spin densities,[99] and the nature of ligands. In addition to the capability of

distinguishing between ligands with similar atomic number (e.g., C, N, O) or different protonation states of the ligands, which cannot be achieved by EXAFS, another important advantage of XES is that the experiments do not require ultra-high vacuum (UHV) and allow for measurements under *in situ* or *operando* conditions in more complex environments.[100]

Non-resonant valence-to-core XES (vtc-XES) can in principle be implemented at any X-ray beamline or laboratory source that is equipped with X-ray spectrometers, as it does not require monochromatic radiation because of the excitation into a continuum level.[100] While vtc-XES has found prevalent use in 3d transition metal systems, valence-to-core transition features of 4d and 5d transition metal compounds are poorly resolved occurs on a picosecond timescale. This is reflected in a recent study on X-ray pulse-induced effects on the chemical state of the catalytically relevant redox center in two Mn complexes in water, by taking $K\beta_{1,3}$ XES spectra under ambient conditions.[101] The liquid jet technique was used, and the solution samples were injected into the X-ray probe in the chamber by means of an electrohydrodynamic liquid jet of several μm thickness at the interaction region using the cone-jet mode.[101] Here, a very thin and fast electrospun microjet produced from a gas dynamic virtual nozzle was used to generate a stream of monodisperse and stable droplets.

3.3 X-ray photoelectron spectroscopy (XPS)

The vacuum liquid microjet technique (Fig. 9a), in combination with high brilliance synchrotron radiation and a differentially pumped analyzer placed close to the sample surface, has enabled *in situ* applications of surface-sensitive XPS in aqueous environments and at contaminant-free interfaces.[102]

Two types of *in situ* XPS studies pertaining to catalysis have been reported in aqueous solutions, by collecting XP spectra of a specific element from: 1) solvated ions and molecules in water (at the vacuum/water interface[103]); and 2) colloidal NPs in aqueous suspension (at the NP/water or vapour-water-NP interface[104–106]), respectively. No reports have been found in the open literature with respect to *in situ* monitoring of a catalytic reaction in water.

Brown et al. demonstrated, using silica NPs, that the surface potential at a water-oxide NP interface, long considered an directly immeasurable quantity, can be measured by XPS.[105] It was envisioned that the surface potential at solution-oxide interfaces of mixed colloidal systems can be simultaneously determined for each type of particles. These authors also found that the increased negative surface charge density of smaller silica colloids at high pH results in a preferential exclusion of the particle from the vapour-water interface.[106]

Note, however, that NP suspensions represent a challenge for expansion through the liquid microjet nozzle with a diameter typically of 20 μm or smaller, due to frequent clogging caused by the higher viscosity and turbidity of such suspensions than pure water.[102f] Therefore, the diameter of the nozzle and, thus, the flow rate of the suspension, have to be increased. Also, the studied liquid is not in thermodynamic due to substantial core-hole life-time broadening. By taking advantage of resonant inelastic X-ray scattering (RIXS), where the broadening of the spectral features is mainly due to the instrumental energy bandwidth, this problem can be overcome, thus enabling elucidation of electronic structures of these materials.

XES benefits more than XAS from the development of X-ray free electron lasers (XFELs).[101] Traditionally, XES spectra of most redox-active aqueous systems are collected under cryogenic conditions to trap the chemical intermediates and avoid radiation damage to them. Now, the ultrashort femtosecond X-ray pulses of XFELs in a shot-by-shot mode can avoid radiation damage caused by radical diffusion, which equilibrium and gaseous contributions to the spectra have to be carefully considered.

An alternative design of the *in situ* XPS apparatus for aqueous systems uses a 15 nm thick Si membrane in a 100 μm thick Si frame to separate vacuum from ambient solution; the total photoelectron signal contains those generated on both sides of the membrane (Fig. 9b).[107] A quantitative analysis, based on the Si 2p XPS peak intensities, of the EC growth of Si oxide was conducted in real time at varying potentials. Here, the weakness is that the cell-volume has to be minimized to prevent any membrane damage due to the pressure gap between the inside and outside of the cell. The Si_3N_4 or Si membrane also has to be very thin (e.g., 15 nm for Si_3N_4) to allow photoelectrons to be detected by XPS.

4. Synchrotron-based X-ray diffraction and scattering

Although X-ray diffraction (XRD) and scattering were not extensively used to monitor the structure alterations of catalysts in aqueous systems, synchrotron high-energy X-rays, representing a class of promising probes for solution-phase reactions due to their strong penetration in liquids and weak absorption in reactants, have enabled diffraction or scattering studies that probe phase evolution of colloidal nanoparticles, in ambient, hot or supercritical liquids.[108–110]

As a recent example of *in situ* monitoring of aqueous phase synthesis of metal colloids,[111] time-resolved XRD patterns were recorded with 10 s (even shorter is possible) exposure of the beam to a $AgNO_3$-glycerol-PVP solution, to capture the nucleation and growth events of Ag nanowires. Analysis of the phase transition kinetics and reaction thermodynamics pinpointed the fact that the fragmentation of the nanowires stems from the instability of the nanowire surface lattices at elevated temperatures.[111] In this case, the setup allowed collecting scattered X-ray signals up to 2θ of ca. 13° and over a full range of orientations perpendicular to the X-ray beam.

Small-angle X-ray scattering (SAXS), sometimes combined with its wide-angle counterpart (WAXS), is a proven method for monitoring the formation and growth of crystal nuclei of zeolites, zeotypes and other sol-gel nanoparticles from clear aqueous solutions at synthesis temperatures.[112–114] Dynamic light scattering (DLS) measurements serve as a complementary tool, following the crystal growth in large size domains (e.g.,

100−6000 Å) that are beyond the range of the SAXS measurements.[112,115]

Recently, Stavitski et al. reported the first *in situ* combined SAXS/WAXS study on the crystallization process of two aminoterephthalate metal-organic frameworks (MOFs) synthesized from similar metal and organic precursors.[20] Detailed analyses of the kinetic constants and activation energies for nucleation and growth, derived from time-resolved changes of the Bragg reflections, yielded a complete picture of the sequence of events that occur during the crystallization of the two terephthalate-based MOFs in different solvents, i.e., DMF, H_2O and DMF/H_2O mixtures.

Synchrotron SAXS has also been recently applied to investigate nanowetting of superhydrophobic surfaces as well as the morphology of air bubbles trapped inside nanometer-scale hydrophobic cavities,[116] which may find profound implications in catalysis and pertinent diffusion phenomena.

5. Magnetic Resonance Spectroscopy

5.1 Nuclear Magnetic Resonance (NMR) Spectroscopy

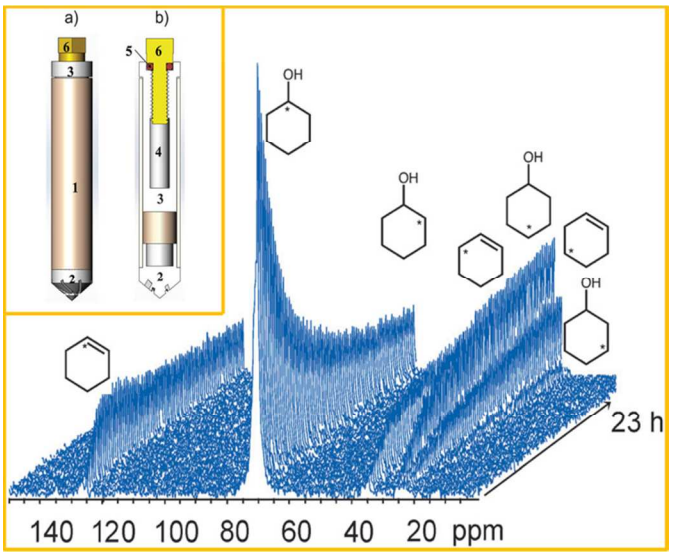

Fig. 10 A stacked plot containing 80 MAS-NMR spectra acquired for a mixture of 22 mg HBEA150 and 120 mL of 0.33 M 1-^{13}C-cyclohexanol at 130 °C in liquid water and as a function of time. The inset shows the design of the 9.5 mm outer diameter high-temperature and high-pressure MAS rotor: (1) the zirconia rotor sleeve, (2) the ceramic insert made of materials such as Macor, (3) the sample cell space and (4) thread, (5) O-ring, and (6) Torlon® screw. The lid of the microautoclave and the valve adaptor to pressurize it, are removable. The outside surface of the insert is fixed to the inner surface of the zirconia rotor sleeve by high-temperature glue. Adapted from ref. 10 with permission. Copyright 2014 Wiley-VCH Verlag GmbH & Co. KGaA, Weinheim.

The temporal evolution of reaction intermediates of a homogeneous catalytic reaction in water can be readily followed by solution-phase NMR.[8,9,117,118] Unlike in solution, the presence of anisotropic interactions in NMR spectra of solids generally broadens the spectral lines and thus hinders the extraction of accurate chemical information.[119] Despite the fact that NMR is not intrinsically surface-sensitive, there have been applications of solid-state NMR, specifically, magic-angle-spinning (MAS) NMR, in the study of s-l interfaces and heterogeneous reactions with multiple phases present, typically involving high-surface-area porous or nanostructured materials.[1]

In situ MAS NMR spectroscopy is of great value for both interrogating the state of the catalytic center (e.g., ^{27}Al or ^{119}Sn) and identifying surface adsorbates under working conditions, thereby providing insights into kinetics and reaction mechanisms of heterogeneous catalytic reactions. For such studies, key quests remain to be high spectral resolution, high sensitivity, fast collection of spectra with appropriate S/N ratios, and the ability to satisfy temperature and pressure conditions required by the catalytic reaction. The research progress on the *in situ* solid-state NMR techniques and the applications in heterogeneous catalysis under batch-like and continuous-flow conditions has been described in two recent reviews.[119,120] A topical account of the more recent *in situ* NMR investigations in EC systems was composed by Grey and co-workers.[121]

Here, we highlight two studies that employ chemical structure-induced spectral sharpening[122] and a thoughtfully designed microautoclave rotor,[10] respectively, which allowed obtaining unprecedented information from *in situ* NMR studies in aqueous solutions.

The former study acquired static ^{13}C NMR spectra of formic acid in aqueous colloidal solutions of metal NPs and reported that the measured ^{13}C chemical shifts of adsorbed bridging formate on various metal surfaces correlated linearly with the catalytic activities of these metals in the formic acid decomposition and electro-oxidation in water.[122] Prior efforts had failed to establish such a relationship between adsorption strength and chemical shift values, due to the severely perturbed and broadened ^{13}C chemical shifts caused by Knight-shift effects. This study discovered that the presence of the O spacer atoms in certain adsorbate structures, separating the ^{13}C from direct contact with the metal surface, substantially reduces the Knight-shift effects and eliminates peak broadening.

Many catalytic processes are practised at elevated temperatures and pressures. The design of the MAS NMR rotor, which is used as a microreactor, is crucial for *in situ* investigations under high pressures. Most recently, the potential of the MAS NMR in monitoring multi-phase reactions (solid-liquid-gas in this particular case) under relatively demanding conditions was explored.[10] Here, the rotor was designed to withstand spinning the sample at a rate of 2.4 kHz while allowing operations at pressures up to 20 bar and 200 °C with marginal gas leakage for up to 72 h (see the inset of Fig. 10 for the rotor assembly scheme). The mechanism of the dehydration of aqueous cyclohexanol catalyzed by zeolite HBEA was elucidated through following the isotopomer concentrations (Fig. 10). It was demonstrated that water elimination follows an E1 mechanism forming a cyclohexyl carbenium ion rather than alkoxide species, which either undergoes rapid 1,2-hydride shift or is rehydrated. The slower relaxation of surface bound states was used to differentiate them from mobile species.

5.2 Electron Paramagnetic Resonance (EPR) Spectroscopy

EPR (or ESR, electron spin resonance) spectroscopy, which probes the spin of electrons instead of nuclei, is a less common technique than NMR spectroscopy, partly because it only detects paramagnetic species with unpaired electrons, limiting its versatility. On the other hand, it is inherently roughly three orders of magnitude more sensitive than NMR due to the higher frequency of electromagnetic radiation used in EPR (typically, 3−400 GHz) compared to NMR.

Aqueous solutions or suspensions containing transition metal ions,[123] homogeneous transition metal complexes,[124] heterogeneous Fenton-type catalysts,[125] as well as TiO_2-based photocatalysts,[126−128] have been analyzed by EPR spectroscopy. In particular, photocatalytic systems often involve the generation and reaction of radicals at the surface. A measure of short-lived radical species can be obtained through spin-trapping EPR measurements.

While EPR spectroscopy is a superb tool to detect the EPR-active intermediate formed during a catalytic reaction, the time-dependent evolution of this EPR-active species is not truly *in situ*, as the aqueous solutions are typically frozen, i.e., not at the catalytic relevant conditions, when being analyzed by EPR.

6. UV–Vis spectroscopy

Transmission UV−vis has long been used for investigating liquid precursor media for catalyst preparation, such as aqueous solutions containing homogeneous metal complexes or water-soluble metal colloids. New examples of relevance to catalysis in water keep adding to this application.[9,129−132] A majority of these studies were focused on homogeneous water- or CH-oxidation catalysts; for instance, time-resolved UV−vis spectra shed light on the reactive states of organometallic Ir complexes during catalytic turnovers, showing a rapid and irreversible loss of the cyclopentadienyl ligand.[9]

In contrast, and perhaps surprisingly, *in situ* UV−vis spectroscopy is still not commonly employed to study heterogeneous catalysts in water, either transition metal centers at the surface of catalytic solids, or surface adsorbates (strong chromophores required) at the s-l interface. Even fewer studies reported time-resolved changes in UV−vis spectroscopic features during heterogeneous catalytic reactions in water. If done at all, diffuse reflectance mode is often the choice for such systems.[133]

Free-standing liquid-liquid (l-l) interfaces are ubiquitous in biphasic catalytic and electrochemical systems. Recently, fiber-optic UV−vis spectroscopy was applied to follow the electrodeposition of Au at the l-l interface, induced by ion transfer of a tetrachloroaurate complex from 1,2-dichlorethane (DCE) to the aqueous phase.[134]

A few remarks on the disadvantages of UV−vis, in the context of this review, are needed. First, it gives less distinct information about the molecular structure because of the appearance of rather broad bands. Many species can have transitions in the same wavelength range, so the observed bands may be unspecific. Due to this vagueness in structural identification, it is recommended that it be coupled with techniques more adept at differentiating between plausible structures (e.g., NMR). Second, it is not suitable for measurements of ultrafast processes. Although sub-minute time resolutions are possible for scanning spectrometers, if operated in a single wavelength mode, these spectrometers typically need several minutes to record a spectrum. In contrast, spectrometers with array detectors need less than 10 ms. Third, spectral integration can be challenging due to the broad features, and quantitative analyses are often difficult or even infeasible without another calibration technique, as molar adsorption coefficients are often unavailable.

7. Imaging Techniques: Electron Microscopies, Fluorescence Microscopy, and Imaging Mass Spectrometry

In situ chemical imaging techniques furnish a vivid picture of the dynamically changing structures and ongoing chemical processes in real-space and time. The spatiotemporal imaging of catalysts during reactions is still in its infancy, and represents a vibrant field of research.[2,135a] Complementarily, tomographic reconstruction in a three-dimensional (3D) domain enables the catalyst's micro-/nanostructures to be fully resolved.[135] Despite that some techniques discussed in the previous sections are suitable also for accurate space-resolved studies of heterogeneous catalysts, an example being the dispersive space-resolved (μm scale) XAFS (sorted into the X-ray scanning microscopy category),[67] they may be so time-consuming that time resolution is not available.

Recent work on chemical imaging at synchrotron sources of catalytic solids was reviewed.[136] Next, we briefly survey recent advances and applications of representative imaging techniques at s-l interfaces relevant to catalysis in water. A comprehensive summary of all relevant techniques[1] is out of the scope of this review.

7.1 Electron microscopies (EM)

Over the past decade, tremendous research efforts have been dedicated to liquid-cell electron microscopies, primarily TEM and STEM, for studying NP growth in liquid water and other solvents.[137] A well-sealed liquid cell can maintain a small amount of liquids inside the cell for an extended period of time under high vacuum.[138] An electric bias can be readily applied between two electrodes in such a liquid cell for the in situ electrochemical TEM experiments. Owing to the advances in fluid stages and microfabrication, imaging liquids in EMs is becoming routine. Liquid microfluidic cells used for *in situ* electron microscopy have been summarized in a recent review.[139] Note that the use of *in situ* TEM was just recently extended to imaging the motion of organic, polymeric soft nanomaterials in liquid water,[140] implying that fewer constraints will remain with regard to the type of catalytic materials that can be characterized by this approach. However, no *in situ* TEM observations of changes with catalytic materials at work have been reported in the aqueous phase. One of the current

limitations of *in situ* TEM cell is such that the spacing between the two window membranes of the TEM cell generally does not exceed ca. 200 nm in order to allow the electron beams to pass through the loaded solution for optimal imaging, precluding studies of materials with dimensions larger than the spacing of the cell windows.[141]

7.2 Transmission X-ray microscopy (TXM)

Although the spatial resolution of TXM is much lower than that of EM techniques, it offers several unique advantages over EM, including image contrast control by tunable X-ray energy and significantly reduced operational constraints owing to the large penetration depth of X-rays,[141] thus permitting *in situ* studies fully compatible with liquid-phase reactions. Here, hard X-ray microscopy experiments in the micron range are very interesting for catalysis as the hard X-rays allow realistic catalytic conditions and the detection of the 5d elements.[142]

The flow-cell TXM technique was employed for observing the morphological evolution of Ag nanowires in the course of a galvanic replacement reaction with an aqueous solution of $HAuCl_4$ at room temperature.[141] The use of a flow cell allows triggering the reaction by delivering a $HAuCl_4$ solution into the cell once the TXM is ready for imaging. Reaction chambers as thick as hundreds of micrometers (*vs.* several hundred nanometers in TEM) enable easy manipulation of nanowires (~10 μm length).[141] Multiple steps associated with the chemical transformation of solid Ag nanowires into hollow Au or Au-Ag nanostructures were visualized.

7.3 Fluorescence microscopy (FM)

Single-molecule fluorescence imaging, in which fluorescent reaction products are imaged and localized precisely one at a time to achieve tens-of-nanometer resolution in resolving catalytic reactions, has emerged as a powerful imaging technique for revealing spatial distribution of chemical reactivity on surfaces, the phase of active catalysts and reaction mechanisms.[11,143–146] For instance, it has proved very useful for differentiating between homogeneous and heterogeneous pathways potentially available for a reaction occurring in solution phases.[143] In the aqueous phase, the fluorophore probe, which is presently typically at very low concentrations (e.g., 10^{-12} M), needs to be water-soluble or hydrophilic at one of its ends.[146] These probes were applied to the *in situ* observation of interfacial electron-transfer events, including molecular adsorption and desorption of organics, upon UV irradiation of TiO_2 nanorods and NPs.[145,146] Scopes and limitations of FM in the applications to study catalysis have been discussed in recent reviews.[147,148]

In a most recent example of super-resolution fluorescence imaging, Chen and colleagues were able to differentiate and quantify directly the catalytic activity at the corner, edge, and facet regions on single mesoporous SiO_2-coated 2D Au nanoplates in catalyzing the reductive N-deoxygenation of resazurin to resorufin (Fig. 11).[11] On a single Au nanoplate, it was directly visualized that the specific activity follows the trend of corners > edges > flat surface facets (Fig. 11c). When averaged over many Au@mSiO_2 nanoplates, this trend persists, with the specific activity of the corner region being ca. 8% higher than the edge region, which in turn is almost twice as high as the flat facet region (Fig. 11d).

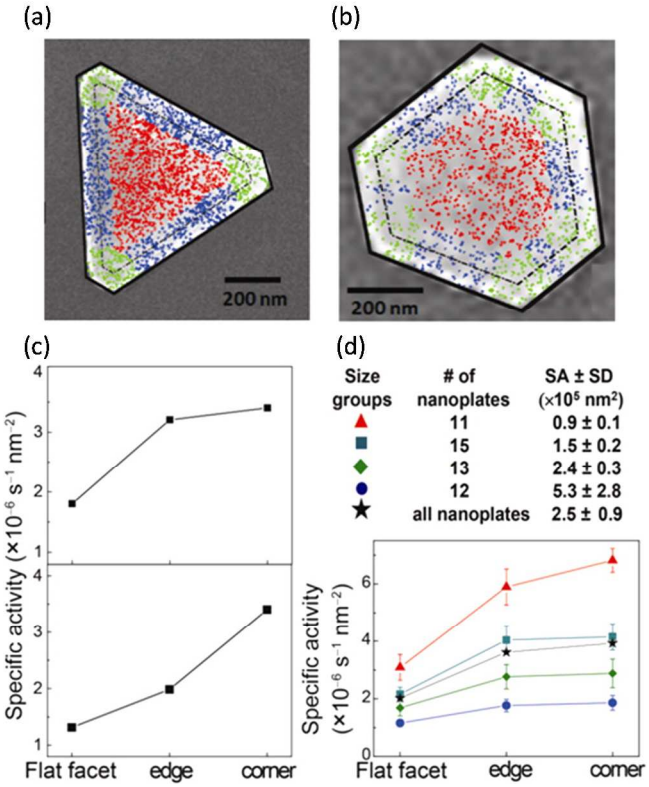

Fig. 11 Spatially resolved activity quantitation on single Au@mSiO_2 nanoplates. (a) Locations of 2325 product molecules overlaid on top of the SEM image of an Au@mSiO_2 nanoplate. Each dot is the location of one product molecule. The locations are colour coded according to their respective regions on the nanoplate: flat facet (red), edges (blue), and corners (green). The solid black line outlines the outer contour of the mSiO_2 shell. The dashed black line outlines the perimeter of the Au nanoplate core. (b) Same as (a) but for a different Au@mSiO_2 nanoplate with 1579 products detected. (c) Specific activities of the different regions of the nanoplates from (a, top) and (b, bottom). (d) Averaged specific activities of different regions on the nanoplates for different size groups (SA = surface area) as well as for all the nanoplates. Error bars represent standard deviations. Adapted from ref. 11 with permission. Copyright 2013 American Chemical Society.

7.4 Scanning Probe Microscopies

To image s-l interfaces with subnanometer (or even atomic) resolution, the most promising approach is the use of scanning microscopies, primarily scanning tunnelling microscopy (STM) and atomic force microscopy (AFM). Compared with SEM and TEM, STM and AFM provide a three-dimensional surface profile, and they do not typically suffer from charging artifacts in the final image, and are perfectly applicable to ambient and liquid environments. Instead, artifacts in the latter two techniques are mainly related to probe motion and geometrical considerations of the tip-surface interaction. The features and applications of these techniques have been reviewed recently at s-l interfaces.[1] We present below a concise update of, along with a few comments on, each technique pertaining to catalytic

materials in water and aqueous catalytic chemistry. Integration of STM and AFM with other optical techniques (such as IR and fluorescence microscopy) is definitely possible and attractive, but examples are still scarce in relation to aqueous catalytic systems.

STM at s-l interfaces requires, preferably, the use of nonpolar liquids, as the currents originating from the flow of polar molecules (e.g., water) or dissolved ions can be large enough to prevent detection of the tunnelling current. To overcome this effect, a common practice in aqueous phase electrochemical STM studies has been to coat the tip, except for the very end, with an insulating material.[1] Owing to this modification, STM imaging in aqueous electrolyte and under electrochemical reaction conditions has become viable and now forms an active area of research. In a majority of recent work, self-assembled supramolecular structures, ranging from π-conjugated macromolecules to chiral calixarenes, have been identified *in situ* at aqueous/Au(111) interface, during electrochemical reactions[149,150] or without electrochemical potential applied.[151] Notably,[152] STM combined with electrochemical measurements and DFT calculations were used to establish the relationship between the activity for the electro-oxidation of CO in a CO-saturated aqueous solution and the morphology of steps at single-crystal Pt(111) electrode surfaces. The key observation was that the cause for the extremely high catalytic activity of the pristine, disordered (111) step is the presence of poorly coordinated Pt step-adatoms, which not only severely disrupt the protective CO adlayer but also possibly function as catalytic sites.[152] Down the road, more diverse catalytically relevant adsorbate structures are yet to be explored by *in situ* STM in the aqueous phase.

As to time resolution, recording a standard image typically takes about several tens of seconds for a standard STM, down to a fraction of a second for a fast scanning STM. For some catalytic processes, this time resolution is not really sufficient for real-time observations. In this respect, the playmaker will be high speed and time-resolved STM (atom-tracking, open feedback loop), which can gain several orders of magnitude higher time resolution.[153]

AFM is ideal for making *in situ* observations of nanometer-sized features on growing crystal surfaces to disclose three-dimensional details of the assembly process.[154] Anderson and co-workers pioneered in applying *in situ* AFM to reveal key aspects in the dissolution of industrially important LTA[155] and LTL-type[156] zeolites in liquid water. Dissolution rates and activation energies were determined at close to room temperature. Importantly, the tip of AFM may aid in crystal dissolution.[156] In their recent work,[18] the growth of a microporous zincophosphate sodalite crystal was monitored *in situ* by AFM in synthetic parent solutions, which helped the authors revisit some of the axioms governing crystal growth of nanoporous framework solids (including the more important aluminosilicate zeolites) in general. Interestingly, it was noted that the substantial lateral deflection registered specifically at the point of the surface that was growing or dissolving could be used to evaluate the energy imparted to the tip from the crystal growth process at the surface.[18] In these studies, experiments were carried out in the contact mode; while noncontact and tapping modes, where the cantilever is vibrated, may serve to obtain additional information on the forces at play.

By and large, the lateral resolution obtained through AFM imaging is an order of magnitude less than the vertical resolution; this is due, in part, to the fact that the observed cross-sectional profile of any step edge is a convolution of the AFM tip shape and the actual structure of the step edge being imaged. With this limitation present, cross-sectional analyses of the step edges, as shown by Moh et al.,[154] may provide insights into details of crystal growth at the lateral dimension.

7.5 Imaging mass spectrometry

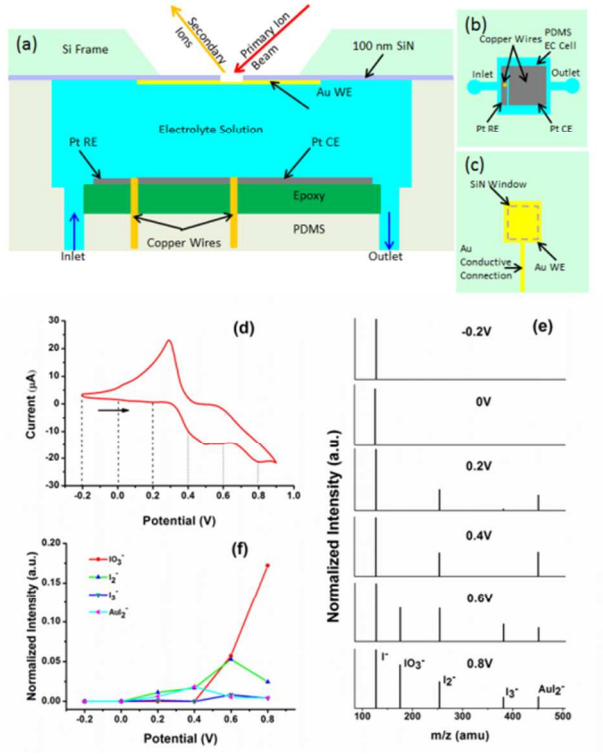

Fig. 12 The microfluidic EC device for ToF-SIMS analysis including (a) a schematic of the side view of the device, (b) the top perspective of the Pt as CE and RE, (c) the top perspective of the Au WE; (d) the cyclic voltammogram for the polycrystalline Au electrode in 10 mM KI at a scan rate of 100 mV s^{-1} (ranging from -0.2 V to 0.9 V, starting at -0.2 V); (e) m/z spectra (only m/z peaks of interest are shown) acquired at -0.2 V, 0 V, 0.2 V, 0.4 V, 0.6 V, and 0.8 V, respectively; (f) normalized intensity from the m/z spectra obtained by ToF-SIMS as a function of potential. The I^- signal was used as a reference for normalization of each spectrum. Adapted from ref. 161 with permission. Copyright 2014 Royal Chemical Society.

To date, imaging mass spectrometric tools have been developed to spatially map (x-y scanning) the *in situ* changes in signal intensities of a specific signature.[2,157] The recent works by Yu and co-workers, who took advantage of imaging capabilities of time-of-flight secondary-ion-mass-spectrometry (ToF-SIMS), are worth mentioning. ToF-SIMS is a surface sensitive imaging tool. Similar to XPS, it is a vacuum technique. However, instead of providing information on chemical state, ToF-SIMS

can provide molecular identification with high sensitivity. Therefore, it has been widely used in materials science and increasingly so in biological sciences as well. A portable microfluidic device was designed to be vacuum-compatible and adaptable to more than one analytical platform. The microfluidic reactor was composed of a 100 nm thick Si_3N_4 membrane and PDMS microchannel. During surface analyses, an aperture of 2−3 microns in diameter is drilled through the Si_3N_4 and subsequently exposes the aqueous solutions directly to the probe beam.[139,158] Surface tension is used to hold the liquid within the open detection window. The device can sustain high vacuum ($< 5\times10^{-7}$ mbar) conditions and provide reproducible measurements for up to 8 h.[158–160]

A new advanced EC microchip incorporates a three-electrode system consisting of a Au WE, Pt CE and Pt reference electrode (RE) (Fig. 12).[161] The m/z spectra and 2D images of a specific m/z, taken at different potentials, clearly showed that the elemental/molecular composition and spatial distribution of the reaction products and intermediates at different stages of the EC redox cycle can be monitored and imaged *in situ* using ToF-SIMS.[161] It was also shown that the EC potential for a species to form at the electrode-electrolyte interface can differ from what would be expected from its standard redox potential, further elucidating the importance of real-time kinetic observations of complex solid-electrolyte interfaces. It is perceivable this technique can be applied to study s-l interfaces of interest in heterogeneous electrocatalysis.

8. A short note on other techniques

This review is not intended to encompass all characterization methods applicable to *in situ* monitoring of catalytic processes and related phenomena in the aqueous phase. Instead, it aims to provide an update to major techniques and emerging methods which have attracted more research activity over the past five years. A few potentially useful techniques, while powerful in some aspects, have not seen much *in situ* use or progress in this respect, and are therefore not reviewed in this contribution. Mössbauer spectroscopy is one example, which is largely limited to solid samples or frozen solutions. Although the Mössbauer effect in liquid may become detected at room temperature or above, if the liquid is confined in microcavities of certain mesoporous silicate glass of a mean pore diameter of ca. 4 nm.[162] However, this variant capillary Mössbauer spectroscopy seems to have attracted little interest from the catalysis community. The reason could be the much lower intensity compared with solid samples, if at all observed. In addition, the Lamb-Mössbauer factor for certain nuclei (Sn^{II}), in aqueous solutions or liquids in general, may result in the complete disappearance of Mössbauer pattern well below room temperature.[163]

9. Concluding Remarks and Outlook

Growing interests in conducting the catalytic reaction in the inexpensive, abundant and environmentally benign aqueous media have stimulated the invention and development of a multitude of characterization methods for *in situ* and time-resolved investigations of aqueous phase catalysis. Although we have shown that electrocatalytic systems are currently under the most intensive investigations, the scope of reactions and catalysts subject to such studies is expected to rapidly expand over next decades. Conventional technical constraints in applying spectroscopic and microscopic techniques to aqueous-phase catalytic systems have been significantly overcome, owing to ingenious designs that, for instance, minimize the paths that the probe beam (e.g., electrons) need to travel through the aqueous phase, or that employ unique surface phenomena for more practical substrates and surfaces (e.g., SERS and SHINERS). More realistic temperature and pressure conditions are starting to be used, thereby closing the knowledge gap between real-world catalysis and more idealistic model systems.

Massive efforts have been devoted to pushing spatial and temporal resolutions. To monitor relatively fast kinetics, an ideal scenario would be an as-short-as-possible sampling and recording time without considerably compromising S/N ratios. This is not easily achievable, for instance, in MAS NMR, as bigger rotors and higher spinning rates, both serving to improve S/N ratios, go against each other in practical operations. With many techniques used for time domain studies, compromises are currently made between spectral and kinetic time resolution, and this represents an area where profound improvements are warranted.

A majority of examples reviewed in the foregoing sections reported qualitative observations. While quantification attempts have proven successful for many spectroscopic methods and have generated valuable kinetic information, it is not a trivial task for some techniques, e.g., SFG, due to the complexity in data interpretation. To better understand catalysis, it is imperative that a series of reliable, quantitative, and, preferably, straightforward relationships–most importantly, between signal intensities and absolute/relative concentrations of species–be established for individual techniques. As an example, some of the experimental factors that require further analyses for achieving fully quantitative results in the liquid (S)TEM, such as electron dose, liquid thickness, accelerating voltage, have been identified.[164]

Future research directions can be envisioned, including the following: 1) *in situ* SERS studies of various metal-catalyzed reactions in water will continue to grow, considering the ever-increasing number of superior substrates both catalytically and SERS-active, as well as simple, low-cost and innovative substrate fabrication methods.[165] This is one of the exciting loci where discoveries in material sciences can directly serve applications in catalytic sciences; 2) the shell-isolated strategy is in principle extendable to other active substrates for surface enhanced spectroscopies,[53] and will also attract more attention from the catalysis community, primarily because of its practical applicability to materials with diverse dimensions and morphologies; 3) in view of the increasing application of SFG in model electrocatalytic systems, it is also promising that

SFG/SHG studies that monitor real-world multiphase heterogeneous catalysis in the aqueous environment, *in situ* and in a time-resolved manner at elevated temperatures and pressures, will soon emerge; 4) broken-symmetry-specific SFG/SHG techniques are also suited for studying nanoscale chiral structures[166] in advanced materials for heterogeneous enantioselective/chiral catalysis in water; 5) as one of the few techniques that probe oxidation states of elements at the surface, XPS studies of catalytic solid surfaces at work in liquid water are yet to come; 6) valence-to-core XES techniques will attract ever increasing attention, particularly in transition metal systems (coordinated with small atomic-number atoms such as C, N and O) in pressurized and liquid environments;[100] 7) as thoughtfully assessed and compellingly demonstrated by Seidler et al.,[167] a large body of contemporary X-ray based research on catalytic and energy storage systems can be tremendously facilitated by the development of laboratory-based instruments (e.g., Rowland-circle monochromators), thereby replacing the need to perform X-ray spectroscopic measurements exclusively at less accessible, less convenient and oftentimes overpowering synchrotron high-brilliance light sources; 9) *ab initio* calculations and molecular dynamics simulations will play an increasingly important role in rationalizing and interpreting *in situ* observations of aqueous phase catalysis and related adsorption phenomena.[168]

The toolbox for characterizing heterogeneous catalysis in water is still expanding. In space domains, more single-particle and single-molecule detection methods are emerging. In this regard, the spatial resolution shown in Fig. 1 does not represent the highest value achievable to date with each technique. For instance, sub-nm spatial resolution was recently achieved with TERS (conventionally, with 3−15 nm spatial resolution) at the plasmonic junction of a STM, resolving the inner structure and surface configuration of a single molecule.[169] A recent study employed plasmonic spectroscopy to probe, with single-NP resolution, the dynamics of a Galvanic exchange reaction and identified a critical structural event in the transformation; the results gravely questioned the prevalent use of ensemble-averaged kinetics.[170] Submicrometer and nanometer X-ray beams and associated techniques, such as micro-XANES, promise improved spatial resolution, thereby paving the way for an unprecedentedly detailed level of description of heterogeneous catalyst samples or individual nanostructures.[171]

In time domains, a notable challenge lies in obtaining desirable temporal scales as many elementary reactions of interest occurring in liquids approach that of diffusion limits. Thus fast detection techniques with molecular speciation that can unambiguously determine products and short-lived intermediate species are needed. As ultrafast dynamic techniques in aqueous phases become more accessible,[172] some of these urgent needs may be addressed. Of utmost relevance is the advent of hard X-ray free-electron lasers (XFELs),[173] which begins to revolutionize the field of time-resolved X-ray spectroscopic measurements on ultrafast dynamic processes.

Novel time-resolved techniques based on EM and imaging mass spectrometry can potentially open doors to better determination of complex kinetics in water and other liquids. Dynamic TEM[174–176] and environmental TEM[177,178] are considered to enable direct visualization of structures and processes under controlled atmosphere and water environments, with spatial and temporal resolutions unparalleled by conventional electron microscopies. However, technical challenges such as bulging of the electron transparent membrane windows and precise flow control need to be overcome for time-resolved studies in TEM in general, which is complicated by other challenges intrinsic of EM such as beam damage.

Imaging mass spectrometry, including ToF-SIMS, matrix-assisted laser desorption/ionization (MALDI), and desorption electrospray ionization (DESI), has been widely used in biological systems due to its unique ability of providing molecular-level information on multiple spatial scales.[179] While it is still a novice in catalysis applications, its power of accurate speciation and potential plausibility to time-resolved studies may make it more popular in energy research in the future. Along the same line, techniques developed in multimodal correlative imaging for visualizing complex biological systems (e.g., cells and tissues)[180] could also be utilized for studying catalyst particles ranging from nm to μm, and processes occurring on similar length scales. This also highlights the importance in developing novel mesoscale imaging tools that allow transport of microreactors from one analytical platform to another, linking the microscopic (molecular) and macroscopic (bulk) worlds.

There is no doubt that a combination of several characterization techniques and multifunctional analysis will gain further popularity.[181] To this end, we note that microstructured reactors have been long used in catalysis research, particularly for highly exothermic and fast reactions.[182] Such a miniaturized device that is transferrable among different analytical platforms is greatly needed in heterogeneous catalysis that facilitate characterization and real-time kinetic study across multiple time and space scales. The multichannel design should also enable high-throughput investigations. Compared with batch-type reactors, flow cells often better mimic the operating conditions in heterogeneous catalysis. For instance, liquid NMR imaging coupled with flexible microfluidic reactors[183,184] is desirable, especially at elevated temperatures and pressures.

In summary, the quest for an in-depth understanding of catalytic processes in liquid water has brought forth tremendous technological innovations and will continue to generate more research opportunities. By adapting our characterization toolsets to aqueous phase systems across various space and time domains, this voyage to uncharted territories of aqueous-phase chemistry, while undeniably challenging, is destined to be as rewarding and impactful to the catalysis community.

Acknowledgements

Drs. Shi and Lercher's research is funded by a U.S. DOE Office of Science Basic Energy Sciences (Project No. 47319). Dr. Yu

is grateful to the Pacific Northwest National Laboratory (PNNL) Materials Synthesis and Simulation Across Scales Initiative-Laboratory Directed Research and Development (MS^3-LDRD) fund and the Chemical Imaging LDRD for support. PNNL is operated by Battelle for the DOE under Contract DE-AC05-76RL01830.

Key words

Heterogeneous catalysis, *in situ*, time-resolved, water/aqueous, interface, electrochemical/electrocatalysis

References

1 F. Zaera, *Chem. Rev.*, 2012, **112**, 2920–2986.
2 I. L. C. Buurmans and B. M. Weckhuysen, *Nat. Chem.*, 2012, **4**, 873–886.
3 K. Jiang, K. Xu., S. Zou and W. B. Cai. *J. Am. Chem. Soc.*, 2014, **136**, 4861−4864.
4 J. R. Copeland, G. S. Foo, L. A. Harrison and C. Sievers, *Catal. Today*, 2013, **205**, 49–59.
5 K. N. Heck, B. G. Janesko, G. E. Scuseria, N. J. Halas and M. S. Wong, *J. Am. Chem. Soc.*, 2008, **130**, 16592−16600.
6 Z. A. Chase, J. L. Fulton, D. M. Camaioni, D. Mei, M. Balasubramanian, V. T. Pham, C. Zhao, R. S. Weber, Y. Wang and J. A. Lercher, *J. Phys. Chem. C*, 2013, **117**, 17603−17612.
7 A. Maclennan, A. Banerjee, Y. F. Hu, J. T. Miller and R. W. J. Scott, *ACS Catal.*, 2013, **3**, 1411−1419.
8 M. Nielsen, E. Alberico, W. Baumann, H. J. Drexler, H. Junge, S. Gladiali and M. Beller, *Nature*, 2013, **495**, 85−90.
9 U. Hintermair, S. W. Sheehan, A. R. Parent, D. H. Ess, D. T. Richens, P. H. Vaccaro, G. W. Brudvig and R. H. Crabtree, *J. Am. Chem. Soc.*, 2013, **135**, 10837−10851.
10 A. Vjunov, M. Y. Hu, J. Feng, D. M. Camaioni, D. Mei, J. Z. Hu, C. Zhao and J. A. Lercher, *Angew. Chem. Int. Ed.*, 2014, **53**, 479–482.
11 N. M. Andoy, X. C. Zhou, E. Choudhary, H. Shen, G. K. Liu and P. Chen, *J. Am. Chem. Soc.*, 2013, **135**, 1845−1852.
12 Y. Gorlin, B. Lassalle-Kaiser, J. D. Benck, S. Gul, S. M. Webb, V. K. Yachandra, J. Yano and T. F. Jaramillo, *J. Am. Chem. Soc.*, 2013, **135**, 8525−8534.
13 S. M. Rosendahl, F. Borondics, T. E. May and I. J. Burgess, *Anal. Chem.*, 2013, **85**, 8722−8727.
14 J. Y. Wang, H. X. Zhang, K. Jiang and W. B. Cai. J. *Am. Chem. Soc.*, 2011, **133**, 14876–14879.
15 N. Sivasankar,. W. W. Weare and H. Frei, *J. Am. Chem. Soc.*, 2011, **133**, 12976–12979.
16 M. Zhang, M. de Respinis and H. Frei, *Nat. Chem.*, 2014, **6**, 362–367.
17 T. Yao, Z. H. Sun, Y. Y. Li, Z. Y. Pan, H. Wei, Y. Xie, M. Nomura, Y. Niwa, W. S. Yan, Z. Y. Wu, Y.Jiang, Q. H. Liu and S. Q. Wei, *J. Am. Chem. Soc.*, 2010, **132**, 7696–7701.
18 M. A. Holden, P. Cubillas, M. P. Attfield, J. T. Gebbie and M. W. Anderson, *J. Am. Chem. Soc.*, 2012, **134**, 13066−13073.
19 H. Imai, K. Izumi, M. Matsumoto, Y. Kubo, K. Kato and Y. Imai, *J. Am. Chem. Soc.*, 2009, **131**, 6293–6300.
20 E. Stavitski, M. Goesten, J. Juan-Alcaniz, A. Martinez-Joaristi, P. Serra-Crespo, A. V. Petukhov, J. Gascon and F. Kapteijn, *Angew. Chem. Int. Ed.*, 2011, **50**, 9624 –9628.
21 R. Seidel, S. Ghadimi, K. M. Lange, S. Bonhommeau, M. A. Soldatov, R. Golnak, A. Kothe, R. Könnecke, A. Soldatov, S. Thürmer, B. Winter and E. F. Aziz, *J. Am. Chem. Soc.*, 2012, **134**, 1600−1605.
22 E. Borfecchia, C. Garino, D. Gianolio, L. Salassa, R. Gobetto and C. Lamberti, *Catal. Today*, 2014, **229**, 34–45.
23 F. Zaera, *Chem. Soc. Rev.*, 2014, **43**, 7624–7663.
24 B. L. Mojet, S. D. Ebbesenz and L. Lefferts, *Chem. Soc. Rev.*, 2010, **39**, 4643–4655.
25 T. Burgi and A. Baiker, *Adv. Catal.*, 2006, **50**, 227–283.
26 A. Aguirre, P. A. Kler, C. L. A. Berli and S. E. Collins, *Chem. Eng. J.*, 2014, **243**, 197–206.
27 E. Karabudak, R. Kas, W. Ogieglo, D. Rafieian, S. Schlautmann, R. G. H. Lammertink, H. J. G. E. Gardeniers and G. Mul, *Anal. Chem.*, 2013, **85**, 33−38.
28 S. Hardy, I. M. de Wispelaere, W. Leitner and M. A. Liauw, *Analyst*, 2013, **138**, 819–824.
29 J. Zakzeski, R. J. H. Grisel, A. T. Smit and B. M. Weckhuysen, *ChemSusChem.*, 2012, **5**, 430–437.
30 K. Koichumanova, A. K. K. Vikla, D. J. M. de Vlieger, K. Seshan, B. L. Mojet and L. Lefferts, *ChemSusChem.*, 2013, **6**, 1717–1723.
31 J. Schnaidt, M. Heinen, Z. Jusys and R.J. Behm, *Electrochim. Acta*, 2013, **104**, 505–517.
32 J. Schnaidt, M. Heinen, Z. Jusys and R.J. Behm, *Catal. Today*, 2013, **202**, 154–162.
33 D. Gong, V. P. Subramaniam, J. G. Highfield, Y. Tang, Y. Lai and Z. Chen, *ACS Catal.*, 2011, **1**, 864–871.
34 X. Hu and T. Bürgi, *Appl. Catal. A*, 2012, **449**, 139–144.
35 D. M. Savory and A. J. McQuillan, *J. Phys. Chem. C*, 2013, **117**, 23645−23656.
36 Á. I. López-Lorente, M. Sieger, M. Valcárcel and B. Mizaikoff, *Anal. Chem.*, 2014, **86**, 783−789.
37 C. A. Roberts and I. E. Wachs, *Chem. Soc. Rev.*, 2010, **39**, 5002–5017.
38 F. Fan, Z. Feng and C. Li, *Acc. Chem. Res.*, 2010, **43**, 378–387.
39 H. Kim, K. M. Kosuda, R. P. van Duyne and P. C. Stair, *Chem. Soc. Rev.*, 2010, **39**, 4820–4844.
40 X. Zhu, T. Xu, Q. Lin and Y. Duan, *Appl. Spectrosc. Rev.*, 2014, **49**, 64–82.
41 J. F. Li, Y. F. Huang, Y. Ding, Z. L. Yang, S. B. Li, X. S. Zhou, F. R. Fan, W. Zhang, Z. Y. Zhou, D. Y. Wu, B. Ren, Z. L. Wang and Z. Q. Tian, *Nature*, 2010, **464**, 392–395.
42 P. G. Etchegoin and E. C. Le Ru, *Phys. Chem. Chem. Phys.*, 2008, **10**, 6079–6089.
43 J. Huang, Y. Zhu, M. Lin, Q. Wang, L. Zhao, Y. Yang, K. X. Yao and Y. Han, *J. Am. Chem. Soc.*, 2013, **135**, 8552−8561.
44 E. C. Le Ru, E. Blackie, M. Meyer and P. G. Etchegoin, *J. Phys. Chem. C*, 2007, **111**, 13794–13803.
45 W. Xie, C. Herrmann, K. Kömpe, M. Haase and S. Schlücker, *J. Am. Chem. Soc.*, 2011, **133**, 19302–19305.
46 W. Xie, B. Walkenfort and S. Schlücker, *J. Am. Chem. Soc.*, 2013, **135**, 1657−1660.
47 R. Liu, J. F. Liu, Z. M. Zhang, L. Q. Zhang, J. F. Sun, M. T. Sun and G. B. Jiang, *J. Phys. Chem. Lett.*, 2014, **5**, 969−975.

48 J. Huang, L. Zhang, B. Chen, N. Ji, F. Chen, Y. Zhang and Z. Zhang, *Nanoscale*, 2010, **2**, 2733–2738.
49 C. J. DeSantis, R. G. Weiner, A. Radmilovic, M. M. Bower and S. E. Skrabalak, *J. Phys. Chem. Lett.*, 2013, **4**, 3072−3082.
50 V. Joseph, C. Engelbrekt, J. Zhang, U. Gernert, J. Ulstrup and J. Kneipp, *Angew. Chem. Int. Ed.*, 2012, **51**, 7592–7596.
51 K. N. Heck, B. G. Janesko, G. E. Scuseria, N. J. Halas and M. S. Wong, *ACS Catal.*, 2013, **3**, 2430−2435.
52 S. Kim , L. Piao , D. Han , B. J. Kim and T. D. Chung, *Adv. Mater.*, 2013, **25**, 2056–2061.
53 S. Y. Ding, J. Yi, J. L. Feng and Z. Q. Tian, *Surf. Sci.*, 2015, **631**, 73−80.
54 J. F. Li, S. Y. Ding, Z. L. Yang, M. L. Bai, J. R. Anema, X. Wang, A. Wang, D. Y. Wu, B. Ren, S. M. Hou, T. Wandlowski and Z. Q. Tian, *J. Am. Chem. Soc.*, 2011, **133**, 15922–15925.
55 J. R. Anema, J. F. Li, Z. L. Yang, B. Ren and Z. Q. Tian, *Annu. Rev. Anal. Chem.,* 2011. **4**, 129–150.
56 X. D. Lin, J. F. Li, Y. F. Huang, X. D. Tian, V. Uzayisenga, S. B. Li, B. Ren and Z. Q. Tian, *J. Electroanal. Chem.*, 2013, **688**, 5–11.
57 A. Tittl, X. Yin, H. Giessen, X. D. Tian, Z. Q. Tian, C. Kremers, D. N. Chigrin and N. Liu, *Nano Lett.*, 2013, **13**, 1816−1821.
58 For authoritative reviews, see: (a) Y. R. Shen, *Nature*, 1989, **337**, 519–525; (b) K. B. Eisenthal, *Chem. Rev.*, 1996, **96**, 1343–1360; (c) G. L. Richmond, *Chem. Rev.*, 2002, **102**, 2693–2724; (d) C. D. Bain, *J. Chem. Soc. Faraday Trans.*, 1995, **91**, 1281–1296.; (e) Y. R. Shen and V. Ostroverkhov, *Chem. Rev.*, 2006, **106**, 1140–1154.
59 Z. Lu, A. Karakoti, L. Velarde, W. Wang, P. Yang, S. Thevuthasan and H. F. Wang, *J. Phys. Chem. C*, 2013, **117**, 24329−24338.
60 Y. M. You, A. Bloomfield, J. Liu, L. Fu, S. B. Herzon and E. C. Y. Yan, *J. Am. Chem. Soc.*, 2012, **134**, 4264−4268.
61 R. B. Kutz, B. Braunschweig, P. Mukherjee, R. L. Behrens, D. D. Dlott and A. Wieckowski, *J. Catal.*, 2011, **278**, 181–188.
62 W. T. Liu and Y. R. Shen, *Proc. Natl. Acad. Sci. U.S.A.*, 2014, **111**, 1293–1297.
63 C. M. Thompson, L. M. Carl and G. A. Somorjai, *J. Phys. Chem. C*, 2013, **117**, 26077−26083.
64 A. M. Buchbinder, N. A. Ray, J. L. Lu, R. P. van Duyne, P. C. Stair, E. Weitz, Eric and F. M. Geiger, *J. Am. Chem. Soc.*, 2011, **133**, 17816–17823.
65 C. Y. Wang, H. Groenzin and M. J. Shultz, *J. Am. Chem. Soc.*, 2005, **127**, 9736–9744.
66 M. S. Yeganeh, S. A. Dougal and B. G. Silbernagel, *Langmuir*, 2006, **22**, 637–641.
67 S. Bordiga, E. Groppo, G. Agostini, J. A. van Bokhoven and C. Lamberti, *Chem. Rev.*, 2013, **113**, 1736−1850.
68 In-situ Characterization of Heterogeneous Catalysts, First Edition. Edited by José A. Rodriguez, Jonathan C. Hanson, and Peter J. Chupas. © 2013 John Wiley & Sons, Inc. Published 2013 by John Wiley & Sons, Inc.
69 Y. Yao, Y. Hu and R. W. J. Scott, *J. Phys. Chem. C*, 2014, **118**, 22317−22324.
70 A. F. Lee, P. J. Ellis, I. J. S. Fairlamb and K. Wilson, *Dalton Trans.*, 2010, **39**, 10473–10482.
71 S. A. Tupy, A. M. Karim, C. Bagia, W. H. Deng, Y. L. Huang, D. G. Vlachos and J. G. G. Chen, *ACS Catal.*, 2012, **2**, 2290−2296.
72 A. M. Karim, C. Howard, B. Roberts, L. Kovarik, L. Zhang, D. L. King and Y. Wang, *ACS Catal.*, 2012, **2**, 2387−2394.
73 M. Dreher, B. Johnson, A. A. Peterson, M. Nachtegaal, J. Wambach and F. Vogel, *J. Catal.*, 2013, **301**, 38–45.
74 S. Rabe, M. Nachteggal, T. Ulrich and F. Vogel, *Angew. Chem. Int. Ed.*, 2010, **49**, 6434 –6437.
75 M. Harada and Y. Kamigaito, *Langmuir*, 2012, **28**, 2415−2428.
76 T. Yao, S. J. Liu, Z. H. Sun, Y. Y. Li, S. He, H. Cheng, Y. Xie, Q. H. Liu, Y. Jiang, Z. Y. Wu, Z. Y. Pan, W. S. Yan and S. Q. Wei, *J. Am. Chem. Soc.*, 2012, **134**, 9410−9416.
77 M. W. Kanan, J. Yano, Y. Surendranath, M. Dincă, V. K. Yachandra and D. G. Nocera, *J. Am. Chem. Soc.*, 2010, **132**, 13692−13701.
78 R. S. Khnayzer, M. W. Mara, J. Huang, M. L. Shelby, L. X. Chen and F. N. Castellano, *ACS Catal.*, 2012, **2**, 2150−2160.
79 R. Schiwon, K. Klingan, H. Dau and C. Limberg, *Chem. Commun.*, 2014, **50**, 100−102.
80 H. Imai, M. Matsumoto, T. Miyazaki, K. Kato, H. Tanida and T. Uruga, *Chem. Commun.*, 2011, **47**, 3538–3540.
81 N. Ishiguro, T. Saida, T.Uruga, S. Nagamatsu, O. Sekizawa, K. Nitta, T. Yamamoto, S. Ohkoshi, Y. Iwasawa, T. Yokoyama and M. Tada, *ACS Catal.*, 2012, **2**, 1319−1330.
82 R. K. Hocking, R. Brimblecombe, L. Y. Chang, A. Singh, M. H. Cheah, C. Glover, W. H. Casey and L. Spiccia, *Nat. Chem.*, 2011, **3**, 461–466.
83 D. K. Bediako, B. Lassalle-Kaiser, Y. Surendranath, J. Yano, V. K. Yachandra and D. G. Nocera, *J. Am. Chem. Soc.*, 2012, **134**, 6801−6809.
84 A. Minguzzi, O. Lugaresi, E. Achilli, C. Locatelli, A. Vertova, P. Ghignabc and S. Rondinini, *Chem. Sci.*, 2014, **5**, 3591–3597.
85 J. J. Velasco-Velez, C. H. Chuang, H. L Han, I. Martin-Fernandez, C. Martinez, W. F. Pong, Y. R Shen, F. Wang, Y. Zhang, J. Guo and M. Salmeron, *J. Electrochem. Soc.*, 2013, **160**, C445–C450.
86 D. T. Bowron, E. C. Beret, E. Martin-Zamora, A. K. Soper and E. S. Marcos, *J. Am. Chem. Soc.*, 2012, **134**, 962–967.
87 V. Choudhary, S. H. Mushrif, C. Ho, A. Anderko, V. Nikolakis, N. S. Marinkovic, A. I. Frenkel, S. I. Sandler and D. G. Vlachos, *J. Am. Chem. Soc.*, 2013, **135**, 3997−4006.
88 R. C. Nelson and J. T. Miller, *Catal. Sci. Technol.*, 2012, **2**, 461–470.
89 C. Bressler and M. Chergui, *Annu. Rev. Phys. Chem.*, 2010, **61**, 263–282.
90 E. F. Aziz, M. H. Rittmann-Frank, K. M. Lange, S. Bonhommeau and M. Chergui, *Nat. Chem.*, 2010, **2**, 853–857.
91 P. Wernet, K. Kunnus, S. Schreck, W. Quevedo, R. Kurian, S. Techert, F. M. F. de Groot, M. Odelius and A. Föhlisch, *J. Phys. Chem. Lett.*, 2012, **3**, 3448−3453.
92 J. Singh, C. Lamberti and J. A. van Bokhoven, *Chem. Soc. Rev.*, 2010, **39**, 4754–4766.
93 M. Tada, S. Murata, T. Asakoka, K. Hiroshima, K. Okumura, H. Tanida, T. Uruga, H. Nakanishi, S. Matsumoto, Y. Inada, M. Nomura and Y. Iwasawa, *Angew. Chem. Int. Ed.*, 2007, **46**, 4310–4315.
94 M. A. Newton, *J. Synchrotron Radiat.*, 2007, **14**, 372−381.
95 C. J. Milne, T. J. Penfold and M. Chergui, *Coord. Chem. Rev.*, 2014, **277–278**, 44–68.
96 M. Dell'Angela, T. Anniyev, M. Beye, R. Coffee, A. Föhlisch, J. Gladh, T. Katayama, S. Kaya, O. Krupin, J. LaRue, A. Møgelhøj, D. Nordlund, J. K. Nørskov, H. Öberg, H. Ogasawara, H. Öström, L. G.

M. Pettersson, W. F. Schlotter, J. A. Sellberg, F. Sorgenfrei, J. J. Turner, M. Wolf, W. Wurth and A. Nilsson, *Science*, 2013, **339**, 1302−1305.

97 A. F. Lee, C. V. Ellis, J. N. Naughton, M. A. Newton, C. M. A. Parlett and K. Wilson, *J. Am. Chem. Soc.*, 2011, **133**, 5724–5727.

98 H. H. C. M. Pinxt, B. F. M. Kuster, D. C. Koningsberger, *Catal. Today*, 1998, **39**, 351−361.

99 G. Vanko, P. Glatzel, V. T. Pham, R. Abela, D. Grolimund, C. N. Borca, S. L. Johnson, C. J. Milne and C. Bressler, *Angew. Chem. Int. Ed.*, 2010, **49**, 5910–5912.

100 E. Gallo and P. Glatzel, *Adv. Mater.*, 2014, **26**, 7730–7746.

101 R. Alonso-Mori, J. Kern, R. J. Gildea, D. Sokaras, T. C. Weng, B. Lassalle-Kaiser, R. Tran, J. Hattne, H. Laksmono, J. Hellmich, C. Glöckner, N. Echols, R. G. Sierra, D. W. Schafer, J. Sellberg, C. Kenney, R. Herbst, J. Pines, P. Hart, S. Herrmann, R. W. Grosse-Kunstleve, M. J. Latimer, A. R. Fry, M. M. Messerschmidt, A. Miahnahri, M. M. Seibert, P. H. Zwart, W. E. White, P. D. Adams, M. J. Bogan, S. Boutet, G. J. Williams, A. Zouni, J. Messinger, P. Glatzel, N. K. Sauter, V. K. Yachandra, J. Yano and U. Bergmann, *Proc. Natl. Acad. Sci. USA*, 2012, **109**, 19103–19107.

102 For recent reviews, see: (a) B. Winter and M. Faubel, *Chem. Rev.*, 2006, **106**, 1176–1211; (b) M. A. Brown, M. Faubel and B. Winter, *Annu. Rep. Prog. Chem. C*, 2009, **105**, 174–212.; (c) H. H. Bluhm, *J. Electron Spec. Relat. Phenom.*, 2010, **177**, 71–84; (d) R. Seidel, S. Thürmer and B. Winter, *J. Phys. Chem. Lett.*, 2011, **2**, 633–641.; (e) M. Faubel, K. R. Siefermann, Y. Liu and B. Abel, *Acc. Chem. Res.*, 2012, **45**, 120–130; (f) M. A. Brown, I. Jordan, A. B. Redondo, A. Kleibert, H. J. Wörner and J. A. van Bokhoven, *Surf. Sci.*, 2013, **610**, 1–6; (g) M. A. Brown, A. B. Redondo, I. Jordan, N. Duyckaets, M. T. Lee, M. Ammann, F. Nolting, A. Kleibert, T. Huthwelker, J. P. Mächler, M. Birrer, J. Honegger, R. Wetter, H. J. Wörner and J. A. van Bokhoven, *Rev. Sci. Instrum.*, 2013, **84**, 073904.

103 T. Lewis, M. Faubel, B. Winter and J. C. Hemminger, *Angew. Chem. Int. Ed.*, 2011, **50**, 10178–10181.

104 M. A. Brown, R. Seidel, S. Thürmer, M. Faubel, J. C. Hemminger, J. A. van Bokhoven, B. Winter and M. Sterrer, *Phys. Chem. Chem. Phys.*, 2011, **13**, 12720–12723.

105 M. A. Brown, A. B. Redondo, M. Sterrer, B. Winter, G. Pacchioni, Z. Abbas and J. A. van Bokhoven, *Nano Lett.*, 2013, **13**, 5403−5407.

106 M. A. Brown, T. Huthwelker, A. B. Redondo, M. Janousch, M. Faubel, C. A. Arrell, M. Scarongella, M. Chergui and J. A. van Bokhoven, *Langmuir*, 2013, **29**, 5023−5029.

107 T. Masuda, H. Yoshikawa, H. Noguchi, T. Kawasaki, M. Kobata, K. Kobayashi and K. Uosaki, *Appl. Phys. Lett.*, 2013, **103**, 111605.

108 S. Peng, J. S. Okasinski, J. D. Almer, Y. Ren, L. Wang, W. Yang and Y. Sun, *J. Phys. Chem. C*, 2012, **116**, 11842−11847.

109 M. Rehan, X. Lai and G. M. Kale, *CrystEngComm.*, 2011, **13**, 3725−3732.

110 H. Jensen, M. Bremholm, R. P. Nielsen, K. D. Joensen, J. S. Pedersen, H. Birkedal, Y. S. Chen, J. Almer, E. G. Søgaard, S. B. Iversen and B. B. Iversen. *Angew. Chem. Int. Ed.*, 2007, **46**, 1113–1116.

111 Z. Li, J S. Okasinski, J. D. Almer, Y. Ren, X. Zuo and Y. Sun, *Nanoscale*, 2014, **6**, 365–370.

112 J. N. Watson, L. E. Iton, R. I. Keir, J. C. Thomas, T. L. Dowling and J. W. White, *J. Phys. Chem. B*, 1997, **101**, 10094−10104.

113 E. A. Eilertsen, M. Haouas, A. B. Pinar, N. D. Hould, R. F. Lobo, K. P. Lillerud and F. Taulelle. *Chem. Mater.*, 2012, **24**, 571−578.

114 C. Tyrsted, J. Becker, P. Hald, M. Bremholm, J. S. Pedersen, J. Chevallier, Y. Cerenius, S. B. Iversen and B. B. Iversen. *Chem. Mater.*, 2010, **22**, 1814−1820.

115 A. Aerts, M. Haouas, T. P. Caremans, L. R. A. Follens, T. S. van Erp, F. Taulelle, J. Vermant, J. A. Martens and C. E. A. Kirschhock. *Chem. Eur. J.*, 2010, **16**, 2764–2774.

116 A. Checco, T. Hofmann, E. DiMasi, C. T. Black and B. M. Ocko, *Nano Lett.*, 2010, **10**, 1354−1358.

117 H. Kimura, M. Nakahara and N. Matubayasi, *J. Phys. Chem. A*, 2011, **115**, 14013–14021

118 A. Guerriero, H. Bricout, K. Sordakis, M. Peruzzini, E. Monflier, F. Hapiot, G. Laurenczy and L. Gonsalvi, *ACS Catal.*, 2014, **4**, 3002−3012.

119 S. E. Ashbrook, D. M. Dawson and V. R. Seymour, *Phys. Chem. Chem. Phys.*, 2014, **16**, 8223–8242.

120 W. Zhang, S. T. Xu, X. W. Han and X. H. Bao, *Chem. Soc. Rev.*, 2012, **41**, 192–210.

121 F. Blanc, M. Leskes and C. P. Grey, *Acc. Chem. Res.*, 2013, **46**, 1952–1963.

122 K. Tedsree, C. W. A. Chan, S. Jones, Q. Cuan, W. K. Li, X. Q. Gong and S. C. E. Tsang, *Science*, 2011, **332**, 224–228.

123 E. Ember, H. A. Gazzaz, S. Rothbart, R. Puchta and R. van Eldik, *Appl. Catal. B*, 2010, **95**, 179–191.

124 S. D. Hicks, D. Kim, S. Xiong, G. A. Medvedev, J. Caruthers, S. Hong, W. Nam and M. M. Abu-Omar, *J. Am. Chem. Soc.*, 2014, **136**, 3680−3686.

125 X. Yang, X. Xu, J. Xu and Y. Han, *J. Am. Chem. Soc.*, 2013, **135**, 16058−16061.

126 Z. Wang, W. Ma, C. Chen, H. Ji and J. Zhao, *Chem. Eng. J.*, 2011, **170**, 353–362.

127 R. Chong, J. Li, X. Zhou, Y. Ma, J. Yang, L. Huang, H. Han, F. Zhang and C. Li, *Chem. Commun.*, 2014, **50**, 165−167.

128 A.E. Giannakas, E. Seristatidou, Y. Deligiannakis and I. Konstantinou. *Appl. Catal. B*, 2013, **132–133**, 460–468.

129 O. Metin, S. Sahin and S. Ozkar, *Int. J. Hydrogen Energy*, 2009, **34**, 6304−6313.

130 M. Murakami, D. Hong, T. Suenobu, S. Yamaguchi, T. Ogura and S. Fukuzumi, *J. Am. Chem. Soc.*, 2011, **133**, 11605–11613.

131 J. DePasquale, I. Nieto, L. E. Reuther, C. J. Herbst-Gervasoni, J. J. Paul, V. Mochalin, M. Zeller, C. M. Thomas, A. W. Addison and E. T. Papish, *Inorg. Chem.*, 2013, **52**, 9175−9183.

132 D. B. Grotjahn, D. B. Brown, J. K. Martin, D. C. Marelius, M.-C. Abadjian, H. N. Tran, G. Kalyuzhny, K. S. Vecchio, Z. G. Specht, S. A. Cortes-Llamas, V. Miranda-Soto, C. van Niekerk, C. E. Moore and A. L. Rheingold, *J. Am. Chem. Soc.*, 2011, **133**, 19024–19027.

133 F. Geobaldo, S. Bordiga, A. Zecchina and E. Giamello, *Catal. Lett.*, 1992, **16**, 109−115.

134 Y. Gründer, J. F. W. Mosselmans, S. L. M. Schroeder and R. A. W. Dryfe, *J. Phys. Chem. C*, 2013, **117**, 5765−5773.

135 For recent review, see: (a) J. D. Grunwaldt, J. B. Wagner and R. E. Dunin-Borkowski, *ChemCatChem*, 2013, **5**, 62–80.; (b) H. Friedrich, P. E. de Jongh, A. J. Verkleij and K. P. de Jong, *Chem. Rev.*, 2009, **109**, 1613–1629.

136 A. M. Beale, S. D. M. Jacques and B. M. Weckhuysen, *Chem. Soc. Rev.*, 2010, **39**, 4656−4672.
137 For selected papers and reviews since 2010, see: (a) N. de Jonge and F. M. Ross, *Nature Nanotechnology*, 2011, **6**, 695–704; (b) K. L. Jungjohann, J. E. Evans, J. A. Aguiar, I. Arslan and N. D. Browning, *Microsc. Microanal.*, 2012, **18**, 621–627; (c) K. L. Jungjohann, S. Bliznakov, P. W. Sutter, E. A. Stach and E. A. Sutter, *Nano Lett.*, 2013, **13**, 2964−2970; (d) Y. Z. Liu, X. M. Lin, Y. G. Sun and T. Rajh, *J. Am. Chem. Soc.*, 2013, **135**, 3764−3767; (e) H. G. Liao, K. Y. Niu and H. M. Zheng, *Chem. Commun.*, 2013, **49**, 11720–11727.
138 M. H. Sun, H. G. Liao, K. Y. Niu and H. M. Zheng, *Sci. Rep.*, 2013, **3**, 3227.
139 X. Y. Yu, B. W. Liu and L. Yang, *Microfluid. Nanofluid.*, 2013, **15**, 725–744.
140 M. T. Proetto, A. M. Rush, M. P. Chien, P. A. Baeza, J. P. Patterson, M. P. Thompson, N. H. Olson, C. E. Moore, A. L. Rheingold, C. Andolina, J. Millstone, S. B. Howell, N. D. Browning, J. E. Evans and N. C. Gianneschi, *J. Am. Chem. Soc.*, 2014, **136**, 1162−1165.
141 Y. G. Sun and Y. X. Wang, *Nano Lett.*, 2011, **11**, 4386–4392.
142 F. M. F. de Groot, E. de Smit, M. M. van Schooneveld, L. R. Aramburo and Bert. M. Weckhuysen, *ChemPhysChem*, 2010, **11**, 951–962.
143 N. M. Esfandiari and S. A. Blum, *J. Am. Chem. Soc.*, 2011, **133**, 18145–18147.
144 T. Cordes and S. A. Blum, *Nat. Chem.*, 2013, **5**, 993–999.
145 T. Tachikawa, T. Ohsaka, Z. F. Bian and T. Majima, *J. Phys. Chem. C*, 2013, **117**, 11219−11228.
146 T. Tachikawa, T. Yonezawa and T. Majima, *ACS Nano*, 2013, **7**, 263–275.
147 P. Chen, X. C. Zhou, N. M. Andoy, K. S. Han, E. Choudhary, N. M. Zou, G. Q. Chen and H. Shen, *Chem. Soc. Rev.*, 2014, **43**, 1107–1117.
148 K. P. F. Janssen, G. de Cremer, R. K. Neely, A. V. Kubarev, J. van Loon, J. A. Martens, D. E. De Vos, M. B. J. Roeffaers and J. Hofkens, *Chem. Soc. Rev.*, 2014, **43**, 990–1006.
149 S. Uemura, M. Aono, T. Komatsu, M. Kunitake, *Langmuir*, 2011, **27**, 1336−1340.
150 T. Chen, Q. Chen, X. Zhang, D. Wang and L. J. Wan, *J. Am. Chem. Soc.*, 2010, **132**, 5598–5599.
151 R. Tanoue, R. Higuchi, N. Enoki, Y. Miyasato, S. Uemura, N. Kimizuka, A. Z. Stieg, J. K. Gimzewski and M. Kunitake, *ACS Nano*, 2011, **5**, 3923−3929.
152 J. Inukai, D. A. Tryk, T. Abe, M. Wakisaka, H. Uchida and M. Watanabe. *J. Am. Chem. Soc.*, 2013, **135**, 1476−1490.
153 A. van Houselt and H. J. W. Zandvliet, *Rev. Mod. Phys.*, 2010, **82**, 1593−1605.
154 P. Y. Moh, P. Cubillas, M. W. Anderson and M. P. Attfield, *J. Am. Chem. Soc.*, 2011, **133**, 13304–13307.
155 L.I. Meza, M.W. Anderson, B. Slater and J.R. Agger, *Phys. Chem. Chem. Phys.*, 2008, **10**, 5066–5076.
156 R. Brent, P. Cubillas, S. M. Stevens, K. E. Jelfs, A. Umemura, J. T. Gebbie, B. Slater, O. Terasaki, M. A. Holden and M. W. Anderson, *J. Am. Chem. Soc*., 2010, **132**, 13858–13868.
157 B. M. Weckhuysen, *Angew. Chem. Int. Ed.*, 2009, **48**, 4910–4943.
158 L. Yang, Z. H. Zhu, X. Y. Yu, S. Thevuthasan and J. P. Cowin, *Anal. Methods*, 2013, **5**, 2515–2522.
159 L. Yang, X. Y. Yu., Z. H. Zhu, T. Thevuthasan and J. P. Cowin, *J. Vac. Sci. Technol. A*, 2011, **29**, article no. 061101.
160 L. Yang, X. Y. Yu, Z. H. Zhu, M. J. Iedema and J. P. Cowin, *Lab Chip* 2011, **11**, 2481–2484.
161 B. W. Liu, X. Y. Yu, Z. H. Zhu, X. Hua, L. Yang and Z. Y. Wang, *Lab Chip*, 2014, **14**, 855–859.
162 K.Burger and A. Vertes. *Nature*, 1983, **306**, 353−354.
163 E. G. Bajnóczi, B. Bohner, E. Czeglédi, E. Kuzmann, Z. Homonnay, A. Lengyel, I. Pálinkó and P. Sipos. *J. Radioanal. Nucl. Chem.*, 2014, **302**, 695−700.
164 P. Abellan, T. J. Woehl, L. R. Parent, N. D. Browning, J. E. Evans and I. Arslan, *Chem. Commun.*, 2014, **50**, 4873–4880.
165 J. F. Betz, W. W. Yu, Y. Cheng, I. M. White and G. W. Rubloff, *Phys. Chem. Chem. Phys.*, 2014, **16**, 2224–2239.
166 E. C. Y. Yan, L. Fu, Z. Wang and W. Liu, *Chem. Rev.*, 2014, **114**, 8471–8498.
167 G. T. Seidler, D. R. Mortensen, A. J. Remesnik, J. I. Pacold, N. A. Ball, N. Barry, M. Styczinski and O. R. Hoidn, *Rev. Sci. Instrum.*, 2014, **85**, 113906.
168 H. Wang, A. Sapi, C. M. Thompson, F. Liu, D. Zherebetskyy, J. M. Krier, L. M. Carl, X. J. Cai, L. W. Wang and G. A. Somorjai, *J. Am. Chem. Soc.*, 2014, **136**, 10515−10520.
169 R. Zhang, Y. Zhang, Z. C. Dong, S. Jiang, C. Zhang, L. G. Chen, L. Zhang, Y. Liao, J. Aizpurua, Y. Luo, J. L. Yang and J. G. Hou, *Nature*, 2013, **498**, 82−86.
170 J. G. Smith, Q. Yang and P. K. Jain, *Angew. Chem. Int. Ed.*, 2014, **53**, 2867–2872.
171 G. E. Ice, J. D. Budai and J. W. L. Pang, *Science*, 2011, **334**, 1234–1239.
172 W. M. Liu, F. Y. Han, C. Smith and C. Fang, *J. Phys. Chem. B.*, 2012, **116**, 10535–10550.
173 P. Emma, R. Akre, J. Arthur, R. Bionta, C. Bostedt, J. Bozek, A. Brachmann, P. Bucksbaum, R. Coffee, F.-J. Decker, Y. Ding, D. Dowell, S. Edstrom, A. Fisher, J. Frisch, S. Gilevich, J. Hastings, G. Hays, Ph. Hering, Z. Huang, R. Iverson H. Loos, M. Messerschmidt, A. Miahnahri, S. Moeller, H.-D. Nuhn, G. Pile, D. Ratner, J. Rzepiela, D. Schultz, T. Smith, P. Stefan, H. Tompkins, J. Turner, J. Welch, W. White, J. Wu, G. Yocky and J. Galayda, *Nat. Photonics*, 2010, **4**, 641–647.
174 A. H. Zewail, Science, *Science*, 2010, **328**, 187–193.
175 D. J. Flannigen and A. H. Zewail, *Acc. Chem. Res.*, 2012, **45**, 1828–1839.
176 G. H. Campbell, T. LaGrange, J. S. Kim, B. W. Reed and N. D. Browning, *J. Electron Microsc.*, 2010, **59**, S67–S74.
177 S. Giorgio, S. S. Joao, S. Nitsche, D. Chaudanson, G. Sitja and C. R. Henry, *Ultramicroscopy*, 2006, **106**, 503–507.
178 S. Zhang, L. Nguyen, Y. Zhu, S. Zhan, C. K. Tsung and F. Tao, *Acc. Chem. Res.*, 2014, **46**, 1731–1739.
179 J. D. Watrous and P. C. Dorrestein, *Nat. Rev. Microbiol.*, 2011, **9**, 683–694.
180 B. G. Kopek, G. Shtengel, C. S. Xu, D. A. Clayton and H. F. Hess, *Proc. Natl. Acad. Sci. U.S.A.*, 2011, **109**, 6136–6141.
181 K. S. Krishna, C. V. Navin, S. Biswas, V. Singh, K. Ham, G. L. Bovenkamp, C. S. Theegala, J. T. Miller, J. J. Spivey and C. S. S. R. Kumar, *J. Am. Chem. Soc.*, 2013, **135**, 5450–5456.
182 L. Kiwi-Minsker and A. Renken, *Catal. Today*, 2005, **110**, 2–14.

183 D. L. Olson, J. A. Norcross, M. O'Neil-Johnson, P. F. Molitor, D. J. Detlefsen, A. G. Wilson and T. L. Peck, *Anal. Chem.*, 2004, **76**, 2966–2974.

184 M. Khajeh, M. A. Bernstein and G. A. Morris, *Magn. Reson. Chem.*, 2010, **48**, 516–522.